

Site M0067¹

T. Andrén, B.B. Jørgensen, C. Cotterill, S. Green, E. Andrén, J. Ash, T. Bauersachs, B. Cragg, A.-S. Fanget, A. Fehr, W. Granoszewski, J. Groeneveld, D. Hardisty, E. Herrero-Bervera, O. Hyttinen, J.B. Jensen, S. Johnson, M. Kenzler, A. Kotilainen, U. Kotthoff, I.P.G. Marshall, E. Martin, S. Obrochta, S. Passchier, N. Quintana Krupinski, N. Riedinger, C. Slomp, I. Snowball, A. Stepanova, S. Strano, A. Torti, J. Warnock, N. Xiao, and R. Zhang²

Chapter contents

Introduction	1
Operations	1
Lithostratigraphy	2
Biostratigraphy	3
Geochemistry	4
Physical properties	5
Paleomagnetism	6
Stratigraphic correlation	7
References	7
Figures	9
Tables	26

Introduction

During Integrated Ocean Drilling Program (IODP) Expedition 347, cores were recovered from two holes at Site M0067 (Little Belt), with an average site recovery of 76.7%. The water depth was 23 m, with a tidal range of <10 cm. Existing data sets, including seismic reflection profiles, were evaluated prior to each site to attempt to guide the initial drilling with an anticipated lithologic breakdown. The total time spent on station was 0.36 days.

Operations

Transit to Hole M0067A

Following completion of Hole M0066B, the *Greatship Manisha* commenced transit to Site M0067 (proposed Site BSB-4), located in Little Belt. The vessel commenced transit at 0515 h on 27 October 2013 and arrived on site over Hole M0067A at 0830 h on 28 October.

Hole M0067A

Following arrival, a dynamic positioning model was established and coring operations commenced in Hole M0067A (Table T1). The first piston corer system (PCS) run recovered clay, but subsequent cores consisted of gravel and sand-grade material, which was an unexpected lithology at this depth. While attempting to wash down to 12 meters below seafloor (mbsf) to take a hammer sample, a change in drilling parameters was noted at a depth calculated to be 9.3 mbsf.

At this time (1245 h on 28 October 2013), the winds escalated rapidly and the ship was blown off position, bending the string. The driller was able to trip one pipe off the string and sky the remainder to make the string and vessel safe. The template was brought back on deck, and the drill deck was made secure. Much of the remainder of the day was spent waiting on weather (winds peaked at Force 12 for >4 h).

A total of seven cores were recovered to 9.3 mbsf. Hole recovery was 56.34%.

Hole M0067B

When the winds dropped to safe working levels at 2140 h on 28 October 2013, the vessel repositioned over Hole M0067B, and cor-

¹Andrén, T., Jørgensen, B.B., Cotterill, C., Green, S., Andrén, E., Ash, J., Bauersachs, T., Cragg, B., Fanget, A.-S., Fehr, A., Granoszewski, W., Groeneveld, J., Hardisty, D., Herrero-Bervera, E., Hyttinen, O., Jensen, J.B., Johnson, S., Kenzler, M., Kotilainen, A., Kotthoff, U., Marshall, I.P.G., Martin, E., Obrochta, S., Passchier, S., Quintana Krupinski, N., Riedinger, N., Slomp, C., Snowball, I., Stepanova, A., Strano, S., Torti, A., Warnock, J., Xiao, N., and Zhang, R., 2015. Site M0067. In Andrén, T., Jørgensen, B.B., Cotterill, C., Green, S., and the Expedition 347 Scientists, *Proc. IODP, 347*: College Station, TX (Integrated Ocean Drilling Program).

doi:10.2204/iodp.proc.347.111.2015

²Expedition 347 Scientists' addresses.



ing operations in this second hole began. This hole extended to 10.9 mbsf using a combination of PCS and open holing in an attempt to assess the extent of the gravel. At this depth, the hole was terminated in a gravel and fine sand lithology. This lithology was not anticipated and was therefore not consistent with the scientific aims for the site. Also, the gravel was liable to cause hole stability issues should the hole have continued to greater depth.

A total of five cores were recovered from Hole M0067B to 10.9 mbsf, with one open-hole section. Hole recovery was 97.03% when the open-hole section was discounted.

Lithostratigraphy

The cores recovered from Site M0067 were retrieved from two holes, M0067A and M0067B, drilled to 9.30 and 10.90 mbsf, respectively. The sediments are slightly disturbed in the uppermost 4 mbsf, and deeper lithologic changes presented coring problems, resulting in major core disturbance and reduced core recovery. This resulted in an open-hole advance in Hole M0067B between 5 and 9.5 mbsf. Based on poor recovery and allocations of the recovered material to either optically stimulated luminescence (OSL) dating or palynology/sedimentology offshore, no more cores were described as part of the Onshore Science Party (OSP) deeper than Sections 347-M0067A-3H-1 and 347-M0067B-5H-2.

According to visual core descriptions, Site M0067 is divided into two lithostratigraphic units (Fig. F1). Unit I (0–3.3 mbsf in Hole M0067A and 0–4.42 mbsf in Hole M0067B) is composed of a faintly laminated brown sapropel with millimeter-scale black organic-rich clay laminations and shell fragments, possibly indicating a marine to brackish-marine environment. Unit II (3.3–9.3 mbsf in Hole M0067A and 4.42–10.9 mbsf in Hole M0067B) is a decimeter-scale mixed sand and silt clast-rich unit that most likely represents glacial proximal deposit, with variations associated with ice advance and retreat stages.

Unit I

Intervals: 347-M0067A-1H-1, 0 cm, to 2H-1, 0 cm;
347-M0067B-1H-1, 0 cm, to 2H-2, 38 cm

Depths: Hole M0067A = 0–3.3 mbsf; Hole M0067B = 0–4.42 mbsf

This unit is composed of brown-gray well-sorted clay. The unit is mostly homogeneous with faint millimeter-scale lamination of organic-rich clay and minor bioturbation. There is a strong smell of H₂S, suggesting the presence of sulfidic elements within the core. Some shell fragments and other bioclasts

are present. Core sections were generally well recovered with only slight to occasionally moderate disturbance, particularly at the top of the hole.

The biogenic sulfidic content and low terrigenous fraction of the sediments in Unit I indicate sedimentation in a high-productivity environment and/or a low supply of terrigenous sediment. The fine lamination with an imprint of minor bioturbation and the generally homogeneous character of this brown laminated clay are interpreted as evidence for the establishment of marine to brackish-marine conditions, with low oxygen, to encourage organic matter accumulation.

Unit II

Intervals: 347-M0067A-2H-1, 0 cm, to end of hole;
347-M0067B-2H-2, 38 cm, to end of hole

Depths: Hole M0067A = 3.3–9.3 mbsf; Hole M0067B = 4.42–10.90 mbsf

A gradational boundary from Unit I marks a transition into a gray mixed sediment unit, comprising medium- to coarse-grained sand, silt, and minor clay showing moderate disturbances (Fig. F2). Pebbles ranging from angular to subrounded are present and are up to 1 cm in size. Some clay-rich, centimeter-scale interbeds are present. Clast content increases toward 6 mbsf, where it grades into a poorly sorted gray coarse sandy conglomerate followed by a gravel conglomerate. Clasts include flint, crystalline clasts, limestone, and sandstone. From ~6.3 mbsf, there is a medium-grained, massive gray sand with minor silt content. It is well sorted with biotite, white mica, opaques, and common reworked bioclasts. Around 6.50 mbsf are millimeter- to centimeter-scale black to dark gray crystalline clasts. Clast content decreases greatly deeper than this. The cores in the middle and lower part of this unit are heavily waterlogged, with some mass loss.

The moderately to poorly sorted character of sediments, the polymict clast assemblage, and the abrupt shifts in lithologies in the upper part may indicate deposition in an ice-proximal depositional environment. One possibility may be a proximal outwash plain where braiding of meltwater channels could account for the variation in lithology. Based on the well-sorted nature of the sand in the middle and lower part of Unit II, these deposits may represent a high-energy, fluvial, or deltaic depositional environment, possibly an outwash plain.

The high clast content in the upper part may mark the onset of glacial-proximal deposition. Alternatively, based on the high core disturbance, the clasts may have been transported downhole during the coring process. This would explain the high clast

content at the top of the unit and the fewer dispersed clasts lower in the unit and along the cavities at the edge of the core liner.

Biostratigraphy

Diatoms

At Site M0067, Holes M0067A and M0067B were both sampled at every fine-grained section top for siliceous microfossil analysis. Diatoms were identified to the species level, with the exception of *Chaetoceros* resting spores and vegetative cells, which were only identified to the genus level. A total of 77 diatom taxa were identified at Site M0067 (Tables T2, T3). Diatom taxa were assigned to salinity-based affinity groups based on the Baltic Sea intercalibration guides of Snoeijs et al. (1993–1998). In addition to diatoms, silicoflagellates and chrysophytes were noted. Chrysophytes were grouped into morphotypes. Diatoms were present at all analyzed levels to 3.48 mbsf in Hole M0067A. Diatoms were found to ~4.10 mbsf in Hole M0067B. Samples analyzed deeper than this depth were barren. In both holes, diatoms are considered to be well preserved, based on the preservation of fine structures and gracile diatom species. Quantitative preservational analysis will be undertaken during postcruise research, following Warnock et al. (2007).

All analyzed diatom-bearing samples represent a sub-recent brackish-marine assemblage, typical of the Littorina/post-Littorina Sea stages of Baltic Sea history. This assemblage is typified by *Chaetoceros* resting spores, *Cocconeis scutellum*, *Dimeregramma minor*, *Grammatophora oceanica*, *Paralia sulcata*, *Thalassionema nitzschioides*, and *Thalassiosira eccentrica*. The presence of *Pseudosolenia calcar-avis* and *Thalassiosira ostrupii* in samples from the top of Section 347-M0067B-1H-1 indicates that modern sediment was not recovered, as these species are no longer present in the Baltic Sea (e.g., Snoeijs et al., 1993–1998; Andrén, 2000). The silicoflagellate *Dictyocha speculum* Ehrenberg was found in all samples containing the marine diatom assemblage recorded above. *D. speculum* has been described as requiring a salinity of >20 (Tappan, 1980) but has also been identified in the Black Sea with salinities as low as 10 (McCartney, 1993).

Foraminifers

Results are summarized from the samples taken offshore and onshore (i.e., samples taken from core catchers and regular sections). A total of 21 samples were processed from Holes M0067A and M0067B for the presence of foraminifers (Fig. F3; Table T4).

Site M0067 is located in Little Belt, in a more north-westerly location than Site M0059, and therefore may be expected to show a similar faunal assemblage. However, the recovered foraminiferal fauna is significantly different from that at Site M0059. The two sites also differ markedly in stratigraphy, as Site M0067 has only a ~4 m clay section before transitioning to sand and diamicton (see “**Lithostratigraphy**”), which contrasts markedly with the ~70 m clay section recovered at Site M0059, suggesting either a different depositional setting at the two sites or perhaps also that some erosion may have occurred at Site M0067.

Both agglutinated and calcareous foraminifers were present in Holes M0067A and M0067B. From 0 to ~3 mbsf, *Eggerelloides scabrus* is abundant and is the dominant species, composing 70%–100% of the fauna, with up to 100 specimens per ~20 cm³ sample. Increasing importance of the agglutinated foraminifer *E. scabrus* is generally associated with salinity >17 (Murray, 1991; Frenzel et al., 2005). Between 3 and 4 mbsf, abundance decreases before another maximum occurs in Sample 347-M0067B-2H-2, 12 cm (4.16 mbsf). This sample contains a diverse fauna of nine different species including *Elphidium incertum*, *Ammonia beccarii*, *Elphidium williamsoni*, *Elphidium excavatum* f. *selseyensis*, *Haynesina* sp., *E. scabrus*, *Quinqueloculina* sp., *Elphidium albiumbilicatum*, and *Elphidium excavatum* f. *clavata* (listed in order of abundance). Of the species present, *E. incertum* and *A. beccarii* are the most abundant, with 26% and 18% of the assemblage, respectively. This relatively diverse fauna with a significant contribution of *E. incertum* suggests bottom water salinity of at least 22 (Lutze, 1965; Kristensen et al., 2000).

Ostracods

A total of 21 samples (including 12 core catchers) from Holes M0067A and M0067B were examined for ostracods during the onshore phase of Expedition 347 at the Bremen Core Repository (Germany). Samples were studied in the >125 µm fraction. Ostracods were present in six samples (Fig. F4; Table T5).

Ostracods were found in the interval between 0.21 and 4.17 mbsf (Holes M0067A and M0067B). Abundance of ostracod valves per sediment volume is relatively low (<20 valves/20 cm³ sample) for most of the samples. At ~3.2–3.5 mbsf (Hole M0067A), an abundance peak reaching 50–130 valves/20 cm³ is observed. A total of seven taxa were identified for this site: *Robertsonites tuberculatus*, *Cytheropteron latissimum*, *Elofsonella concinna*, *Sarsicytheridea bradii*, *Sarsicytheridea punctillata*, *Acanthocythereis dunelmensis*, and *Finmarchinella* sp. A relatively low ratio of juvenile valves (30%) suggests that either it was an as-

semblage living in a high-energy environment or that some of the valves are allochthonous (Whatley, 1983). Based on the lithologic description (see “[Lithostratigraphy](#)”), the interval with high ostracod abundance most likely represents a high-energy environment where some redeposition was taking place. The sediments shallower than 3.3 mbsf have high organic matter content, and ostracods are probably dissolved. All of the taxa are shallow-water marine and today are commonly found on Arctic shelves (e.g., Stepanova et al., 2007; Frenzel et al., 2010).

Palynological results

Site M0067 is situated in Little Belt in the southwestern part of the Baltic Sea. The vegetation of the borderlands in that region belongs to the temperate forest zone. Palynological analyses for this site focused on Hole M0067A.

Only two samples from core catchers from Hole M0067A have been analyzed because experience gained from sediments from other sites indicated that only Core 347-M0067A-1H was likely to contain well-preserved in situ palynomorphs. As expected, the core catcher sample from Core 1H contained pollen and other palynomorphs in good preservation and high concentration (~190,000 pollen grains/cm³; Fig. F5; see PalyM0067.xls in PALYNOLOGY in “[Supplementary material](#)”), whereas the core catcher sample from Core 2H was virtually barren of palynomorphs.

The only detailed pollen spectrum from Hole M0067A is dominated by pollen of broad-leaved trees and *Corylus avellana*. The highest percentages were noted for *Quercus* (25%), *Alnus glutinosa* type (20.5%), and *C. avellana* (22%) (Fig. F5, No. 1). Moreover, pollen of other more thermophile trees is present in relatively high amounts: *Tilia cordata* type (Fig. F5, No. 2) and *Fraxinus* (both 3%), as well as *Ulmus* (4.5%) (Fig. F5, No. 3). Fairly low amounts were noted for *Pinus sylvestris* type and *Betula alba* type pollen, at 11.5% and 6%, respectively (Fig. F6). Because of the distinct similarity of this spectrum to the depth interval between 21.86 and 31.95 mbsf in the pollen diagram from Hole M0059A and considering neighboring terrestrial pollen profiles (e.g., Dörfler et al., 2012), the pollen spectrum from the core catcher of Core 347-M0067A-1H may provisionally be correlated with the late Atlanticum/Subboreal periods (~5000 cal. y BP). The age apparently cannot be younger than 2500–3000 cal. y BP, as no *Fagus* pollen has been noted, which around this time is one of the dominating broad-leaved trees in the region (e.g., Dörfler et al., 2012, compare to results for Site M0059). Several remains of aquatic insects are present,

most noteworthy an insect jaw that can be ascribed to the chironomid genus *Cryptochironomus* (Fig. F5, No. 6).

The marine palynomorph assemblage in the sample from Core 347-M0067A-1H is similar to that encountered in some samples from Hole M0059A. Almost 30 organic-walled dinocyst specimens have been identified, of which ~56% belong to the genus *Operculodinium/Protoceratium*. *Lingulodinium* is also present (~22%), with relatively short process lengths averaging 8.5 µm that probably indicate low surface water salinity. The third frequent dinocyst type belongs to the genus *Spiniferites* (~15%) (Fig. F5, No. 4). Cysts of *Gymnodinium* (probably predominantly *Gymnodinium nolleri*) are very frequent and may indicate an age of ~4000 y or younger. Combined with the findings from pollen analyses (e.g., absent *Fagus*), the sample age is probably between 4000 and 2500 y BP. *Gymnodinium* cysts were excluded from the dinoflagellate percentage calculations because of their extraordinary high occurrences: they compose >75% of the total dinocyst assemblage. Foraminiferal test linings are also present in the sample (Fig. F5, No. 5). Combined, the palynological proxies indicate some marine influence, similar to that encountered in the comparable interval from Site M0059, but based on the low dinocyst (excluding *Gymnodinium*) to nonsaccate pollen ratio (value = 0.21) and the presence of aquatic insect larvae and freshwater algae, the terrestrial influence was strong.

Geochemistry

Interstitial water

At Site M0067, five samples were taken from a 4 m interval in Hole M0067A and three samples were collected from an 11 m interval in Hole M0067B. Interpretations of the geochemical data (Table T6) are limited because of the low sampling resolution. However, the observed geochemical variations can be linked to lithology represented by an organic-rich sapropel of marine-brackish origin overlying gravel and sand (see “[Lithostratigraphy](#)” and “[Biostratigraphy](#)”).

Salinity variations: chloride, salinity, and alkalinity

Chloride (Cl⁻) and shipboard salinity measured with a refractometer have very similar patterns and limited variability with depth (Fig. F7A–F7B). Chloride concentrations range 330–350 mM with the exception of a lower value of ~300 mM in the deepest sample in Hole M0067A. Shipboard measured salinity and Cl⁻ based salinity have similar trends represent-

ing brackish values of 19–22 (Fig. F7B–F7C). Alkalinity at Site M0067 is roughly an order of magnitude lower than at nearby Site M0059 (Fig. F7D), with the suggestion of a maximum in the upper organic-rich layer of Holes M0067A and M0067B.

Organic matter degradation: sulfate, hydrogen sulfide, iron, manganese, ammonium, phosphate, pH, bromide, and boron

Pore water sulfate (SO_4^{2-}) concentrations scatter between 2 and 6 mM (Fig. F8A) and are depleted relative to the seawater ratio at this site (Fig. F8B), suggesting degradation of organic matter coupled to SO_4^{2-} reduction. Further evidence for this comes from sulfide (H_2S) concentrations measured for Hole M0067A, which were as high as 2.2 mM (Fig. F8C; Table T6). Extensive H_2S accumulation leading to formation of iron sulfides provides an explanation for low dissolved iron (Fe^{2+}) concentrations that are near the detection limit in the upper part of the sediment. In the underlying sand layer, the only measured Fe^{2+} concentration was 238 μM (Fig. F8D). In contrast to Fe^{2+} , Mn^{2+} was present in the upper 5 mbsf at concentrations of 5–16 μM (Fig. F8E). The moderately high alkalinity, which is linked to organic matter degradation in the upper 5 mbsf, is reflected in correspondingly high ammonium (NH_4^+) and phosphate (PO_4^{3-}) concentrations averaging ~1.7 mM and 0.2 mM, respectively (Fig. F8F–F8G). pH was around 8 in the upper 5 mbsf and slightly dropped to 7.5 at 11 mbsf. (Fig. F8H).

Pore water bromide (Br^-) and boron (B) have concentrations of ~0.55 mM and 400 μM , respectively, in the upper meters of sediment (Fig. F9A, F9C). The Br/Cl and B/Cl ratios are slightly above the seawater ratio, particularly in the uppermost organic-rich clay (Fig. F9B, F9D).

Mineral reactions

Sodium, potassium, magnesium, and calcium

Pore water sodium (Na^+), potassium (K^+), and magnesium (Mg^{2+}) are relatively constant with depth, whereas calcium (Ca^{2+}) increases slightly from 8 to 12 mM (Fig. F10A–F10D). When normalized to Cl⁻, Na/Cl and K/Cl ratios plot near the value for seawater, whereas Mg/Cl is generally above the seawater value and Ca/Cl is consistently above the seawater ratio (Fig. F10E–F10H; Table T7). Together, the element to Cl⁻ ratios indicate little diagenetic alteration of the bottom water Na^+ and K^+ and inputs of Ca^{2+} and Mg^{2+} to the pore water.

Strontium, lithium, dissolved silica, and barium

Strontium (Sr^{2+}) and lithium (Li^+) increase from 20 to 120 μM and from 17 to 21 μM with depth, respectively, whereas dissolved silica (H_4SiO_4) decreases from ~900 to 500 μM with depth (Fig. F11A–F11C). Barium (Ba^{2+}) possibly displays a peak of ~5 μM in the organic-rich sediments similar to alkalinity and NH_4^+ (Fig. F11D).

Sediment

Carbon content

The total carbon (TC) content at Site M0067 varies between 0.2 and 7.6 wt% (Table T8; Fig. F12A). The total organic carbon (TOC) content is comparatively high in the marine-brackish clay of Unit I (0–4.4 mbsf) (Fig. F12B). Deeper than this depth, TOC drops below 0.2 wt%, displaying typical depositional differences between the glaciofluvial to glaciodeltaic deposits and the overlying brackish marine sediments. The total inorganic carbon (TIC) content is low throughout the sediment with values below 1.2 wt% (Table T8; Fig. F12C).

Sulfur content

The total sulfur (TS) content ranges from 0.2 to 2.8 wt%, with low values restricted to the glaciofluvial deposits deeper than 4.4 mbsf (Table T8; Fig. F12D). Similar to the TOC concentrations, the TS values are highest in the marine-brackish deposit of Unit I (upper 4.4 mbsf), indicating increased sulfate reduction rates related to the elevated TOC content and subsequent formation and burial of iron sulfides in the sediments.

Physical properties

This section summarizes the preliminary physical property results from Site M0067. Two holes were drilled at this site. Hole M0067A was drilled to 9.3 mbsf, and Hole M0067B extended to 10.9 mbsf. However, recovery from Core 347-M0067B-5H recorded >250%; it is unknown whether this is due to expansion of the sediments or coring of either fall-down or flow-in sediments or a combination of both. This does influence the results from the lower portion of Unit II, and depths quoted should be treated with caution.

Our analysis focuses on Hole M0067B (Fig. F13), which has the greatest recovery and penetration at this site. However, a combination of PCS and open holing was used for this hole to assess the extent of an unexpected lithology (see “Operations”). All

physical property data from this site are thus sparse and discontinuous.

Natural gamma ray (NGR) increases through lithostratigraphic Unit I, and several meter-scale peaks that might reflect changes in lithology (see “**Lithostratigraphy**”) are observed (Fig. F13). Dry density also exhibits a progressive increase toward the base of lithostratigraphic Unit I. Magnetic susceptibility and noncontact resistivity (NCR) exhibit very little variation with depth in lithostratigraphic Unit I, except for a spike in NCR at ~3 mbsf. At the lithostratigraphic Unit I/II boundary, magnetic susceptibility, NCR, and dry density all abruptly increase. However, only the upper portion of lithostratigraphic Unit II was recovered, and thus no downcore trend for this unit can be inferred. From 9.7 mbsf in the lower interval of lithostratigraphic Unit II, coring operations resumed after an open-hole interval, and similarly high values of magnetic susceptibility and dry density are observed. NCR is generally low, and NGR is highly variable. Deeper than 10.9 mbsf (the official bottom of Hole M0067B), NGR and magnetic susceptibility values increase. We acknowledge that the data plotted appear to extend beneath the base of the hole because of expansion of the sediment/flow-in/fall-down. However, as it was unknown whether the expansion was linear or not, no compression corrections were applied. This will need to be taken into account if these data are used for postcruise analysis.

Paleomagnetism

Magnetic susceptibility measurements and simplified analyses of the natural remanent magnetization (NRM) were made on discrete specimens of standard volume and known mass (see “**Paleomagnetism**” in the “Methods” chapter [Andrén et al., 2015]). A total of 23 discrete samples were taken from Holes M0067A (9 samples) and M0067B (14 samples) at increments of ~50 cm. Magnetic susceptibility (χ) ranged between 0.6×10^{-6} and 1.2×10^{-6} m³/kg in the lower part of Unit II. The χ of the upper part of Unit II and Unit I are low and relatively uniform, $\sim 0.012 \times 10^{-6}$ m³/kg. The intensity of the NRM varied between a maximum of 13×10^{-3} A/m at a depth of ~12 mbsf in Unit II and 0.5×10^{-3} A/m in the bottom part of Unit I. It must be noted here that the measurements presented from Cores 347-M0067B-5H and 6S (9.7 mbsf to base of hole at 10.9 mbsf) are not true depths but apparent depths. Core 5H from 9.7 to 10.70 mbsf recorded 252% recovery, giving an apparent bottom depth of 12.22 mbsf. In line with other disciplines, no compression factor was applied to the data from this interval during initial processing. Measurement depths from Unit I and the upper

part of Unit II (0–9.7 mbsf) are not affected by core expansion.

Paleomagnetic pilot samples were grouped into two categories according to their response to alternating field (AF) demagnetization. The first category, which contains samples from the lower part of Unit II (mostly medium-grained, massive gray sand with minor silt content), is defined by unstable magnetizations. The second category, associated with the upper part of Unit II and Unit I, has a stable magnetic remanence and the inclination agrees with the geocentric axial dipole (GAD) prediction of 71°.

Discrete sample measurements

A total of 23 discrete paleomagnetic samples were obtained from Holes M0067A and M0067B at 25 and 50 cm intervals.

Magnetic susceptibility

The results of the magnetic analyses are shown in Figure F14. Magnetic susceptibility ranges between 0.012×10^{-6} m³/kg (Unit I) and $\sim 1.2 \times 10^{-6}$ m³/kg (Unit II).

Natural remanent magnetization and its stability

The NRM intensity ranges between 0.5×10^{-3} and 12.8×10^{-3} A/m. The restricted number of samples display similar NRM intensities but very different magnetic stability. Only two categories of response to AF demagnetization were observed in the pilot samples (Fig. F15). The pilot sample taken from Unit II at ~10.01 mbsf, which contains medium-grained massive gray sand and minor silt content, displays a linear orthogonal vector that trends toward the origin during AF demagnetization from NRM to 50 mT, and the carrier(s) of remanence have medium to low coercivity, with a residual NRM intensity of ~20% after AF demagnetization at 50 mT. The sample displays erratic behavior at stronger demagnetization levels, and Category 1 samples do not contain a very stable magnetic remanence. The Category 2 pilot sample that represents Units II and I has low coercivity but good paleomagnetic stability. The sample lost 50% of its NRM magnetization at an AF of 20 mT, and the orthogonal diagram also depicts the removal of a weak viscous remanent magnetism (VRM) at low fields (i.e., ~5–10 mT), with a definite univectorial behavior and a linear trend toward the origin.

Paleomagnetic directions

Samples taken from the lower part of Unit II are characterized by scattered and general negative incli-

nations. In contrast, the directions of samples in the upper part of Unit II and Unit I agree well with the predicted GAD inclination values (Fig. F14). We conclude that the geomagnetic field has not been recorded sufficiently well at this site to allow the data to be used for relative paleomagnetic dating.

Stratigraphic correlation

Two holes were drilled at Site M0067: Holes M0067A (9.30 mbsf) and M0067B (10.90 mbsf). Recovery was poor deeper than ~5 mbsf, and reliable correlation downhole from this point was not possible. The meters composite depth (mcd) scale for Site M0067 was constructed by correlating magnetic susceptibility between holes (Fig. F16). Despite its relative proximity to Site M0059, at Site M0067 only a thin fine-grained sediment cover on top of gravels and sands was retrieved. The depth offsets that define the composite section for Site M0067 are given in Table T9 (affine table). For the topmost ~5 mbsf, one splice was created (Table T10).

Seismic units

By integrating seismic data with lithostratigraphy (see “**Lithostratigraphy**”), seismic sequence boundaries were correlated with sediment core and multi-sensor core logger (MSCL) log (magnetic susceptibility) boundaries (Fig. F17). Two-way traveltime values for each lithostratigraphic unit boundary were calculated using sound velocity values measured offshore (see “**Physical properties**”; Table T11).

Seismic Unit I

Two-way traveltime: 0.037 ms

Lithology: faintly laminated sapropel and clay (lithostratigraphic Unit I)

Depth: 0–3.30 mbsf (M0067A), 0–4.42 mbsf (M0067B)

The lower boundary of seismic Unit I coincided with a group of strong reflectors. This seems plausible, as changes in lithology and physical properties data are quite distinctive.

Seismic Unit II

Two-way traveltime: 0.039 ms

Lithology: clast-rich mixed sand and silt (upper part of lithostratigraphic Unit II)

Depth: 3.30–4.80 mbsf (M0067A), 4.42–6.30 mbsf (M0067B)

Seismic Unit II does not correlate with a distinct change in the seismic image. This could be due to uncertainties in the estimated velocity values.

Seismic Unit III

Two-way traveltime: 0.045 ms

Lithology: massive sand with minor silt content (lower part of lithostratigraphic Unit II)

Depth: 6.30–10.9 mbsf (M0067A)

Seismic Unit III correlates with a more massive seismic unit, from which no good physical properties data could be obtained.

References

- Andrén, E., Andrén, T., and Kunzendorf, H., 2000. Holocene history of the Baltic Sea as a background for assessing records of human impact in the sediments of the Gotland Basin. *Holocene*, 10(6):687–702. doi:10.1191/09596830094944
- Andrén, T., Jørgensen, B.B., Cotterill, C., Green, S., Andrén, E., Ash, J., Bauersachs, T., Cragg, B., Fanget, A.-S., Fehr, A., Granoszewski, W., Groeneveld, J., Hardisty, D., Herrero-Bervera, E., Hyttinen, O., Jensen, J.B., Johnson, S., Kenzler, M., Kotilainen, A., Kotthoff, U., Marshall, I.P.G., Martin, E., Obrochta, S., Passchier, S., Quintana Krupinski, N., Riedinger, N., Slomp, C., Snowball, I., Stepanova, A., Strano, S., Torti, A., Warnock, J., Xiao, N., and Zhang, R., 2015. Methods. In Andrén, T., Jørgensen, B.B., Cotterill, C., Green, S., and the Expedition 347 Scientists, *Proc. IODP*, 347: College Station, TX (Integrated Ocean Drilling Program). doi:10.2204/iodp.proc.347.102.2015
- Dörfler, W., Feeser, I., van den Bogaard, C., Dreibrodt, S., Erlenkeuser, H., Kleinmann, A., Merkt, J., and Wiethold, J., 2012. A high-quality annually laminated sequence from Lake Belau, northern Germany: revised chronology and its implication for palynological and tephrochronological studies. *Holocene*, 22(12):1413–1426. doi:10.1177/0959683612449756
- Frenzel, P., Keyser, D., and Viehberg, F.A., 2010. An illustrated key and (palaeo)ecological primer for postglacial to Recent Ostracoda (Crustacea) of the Baltic Sea. *Boreas*, 39(3):567–575. doi:10.1111/j.1502-3885.2009.00135.x
- Frenzel, P., Tech, T., and Bartholdy, J., 2005. Checklist and annotated bibliography of recent Foraminifera from the German Baltic Sea coast. *Stud. Geol. Pol.*, 124:67–86. http://sgp.ing.pan.pl/124_pdf/SGP124_067-086.pdf
- Lutze, G.F., 1965. Zur foraminiferen-fauna der ostsee (The distribution of foraminifera in the Baltic Sea). *Meyniana*, 15:75–142.
- Kristensen, P., Gibbard, P., Knudsen, K.L., and Ehlers, J., 2000. Last interglacial stratigraphy at Ristinge Klint, South Denmark. *Boreas*, 29(2):103–116. doi:10.1111/j.1502-3885.2000.tb01204.x
- McCartney, K., 1993. Chrysophytes: silicoflagellates. In Lipps J.H. (Ed.), *Fossil Prokaryotes and Protists*: Cambridge, MA (Blackwell Sci. Publ.), 143–154.
- Murray, J.W., 1991. *Ecology and Palaeoecology of Benthic Foraminifera*: London (Longman).

- Snoeijs, P., Vilbaste, S., Potapova, M., Kasperoviciene, J., and Balashova, J. (Eds.), 1993–1998. *Intercalibration and Distribution of Diatom Species in the Baltic Sea* (Vol. 1–5): Uppsala, Sweden (Opulus Press).
- Stepanova, A., Taldenkova, E., Simstich, J., and Bauch, H.A., 2007. Comparison study of the modern ostracod associations in the Kara and Laptev seas: ecological aspects. *Mar. Micropaleontol.*, 63(3–4):111–142. [doi:10.1016/j.marmicro.2006.10.003](https://doi.org/10.1016/j.marmicro.2006.10.003)
- Tappan, H., 1980. *The Paleobiology of Plant Protists*: San Francisco (W.H. Freeman).
- Warnock, J., Scherer, R., and Loubere, P., 2007. A quantitative assessment of diatom dissolution and late quaternary primary productivity in the eastern equatorial Pacific. *Deep-Sea Res., Part II*, 54(5–7):772–783. [doi:10.1016/j.dsr2.2007.01.011](https://doi.org/10.1016/j.dsr2.2007.01.011)
- Whatley, R.C., 1983. Some simple procedures for enhancing the use of Ostracoda in palaeoenvironmental analysis. *Norw. Pet. Dir., Bull.*, 2:129–146.

Publication: 20 February 2015
MS 347-111

Figure F1. Graphic lithology log summary, Site M0067. Depths given to represent unit boundaries relate to Hole M0067B.

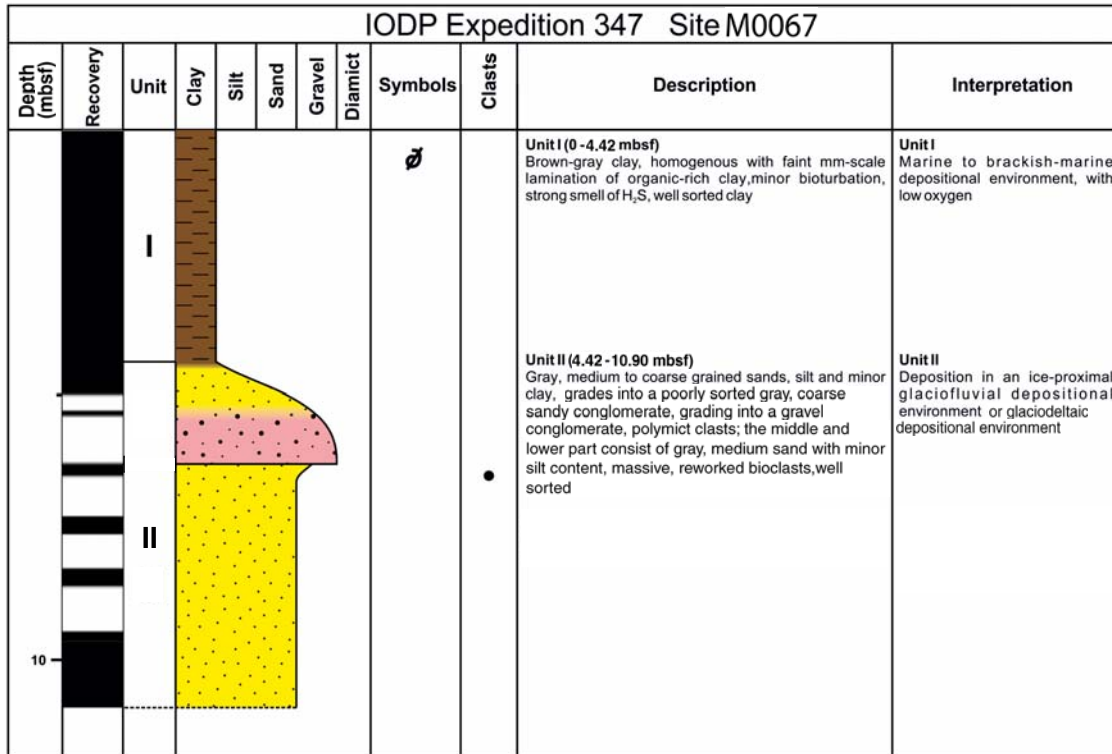


Figure F2. Unit I/II boundary (Core 347-M0067B-2H).

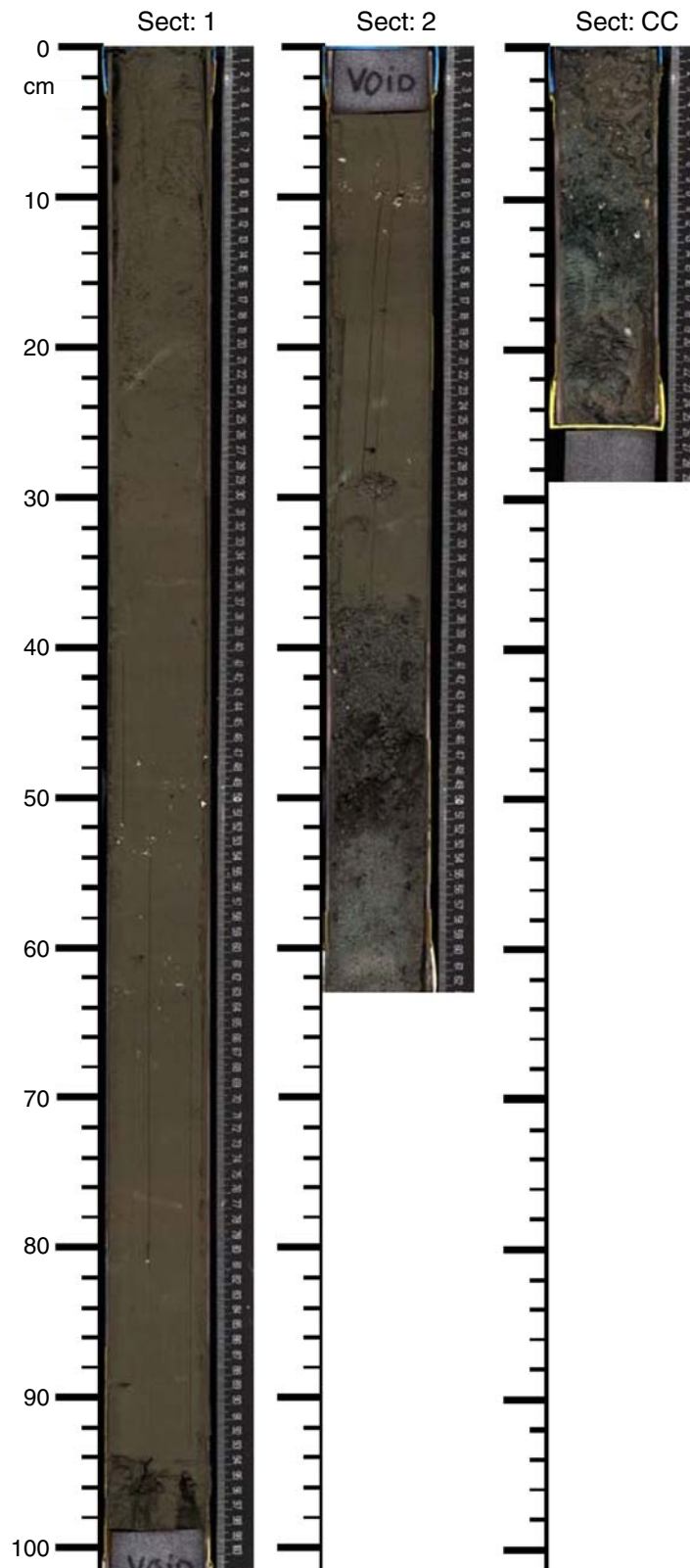


Figure F3. Abundance of benthic foraminifers based on the abundance classification defined in the “**Methods**” chapter (Andrén et al., 2015), Site M0067. Increasing shading indicates abundances sufficient for faunal and/or geochemical analyses.

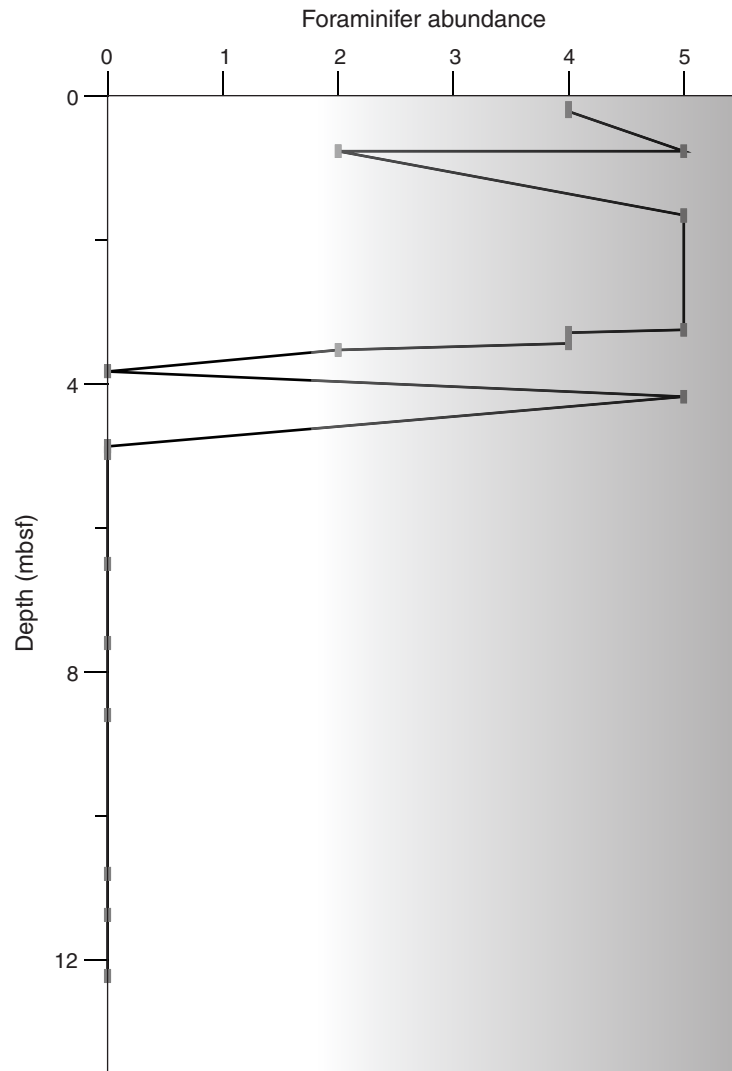


Figure F4. Ostracod abundance per sediment volume, Site M0067.

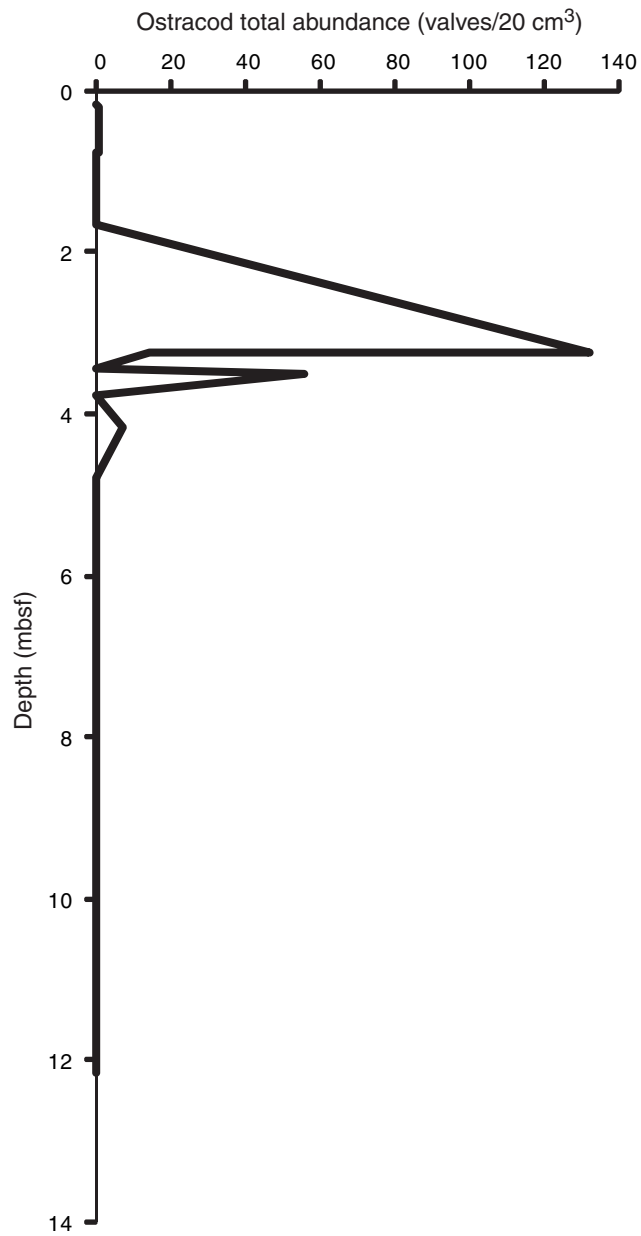


Figure F5. Palynomorphs, Core 347-M0067A-1H. 1–3. Pollen grains, (1) *Corylus* (hazel), (2) *Tilia* (linden), (3) *Ulmus* (elm). 4. Chorale dinoflagellate cyst, *Spiniferites*. 5. Foraminifer test lining. 6. Insect mandible, probably larval chironomid, *Cryptochironomus*. Scale bars = 20 μm .

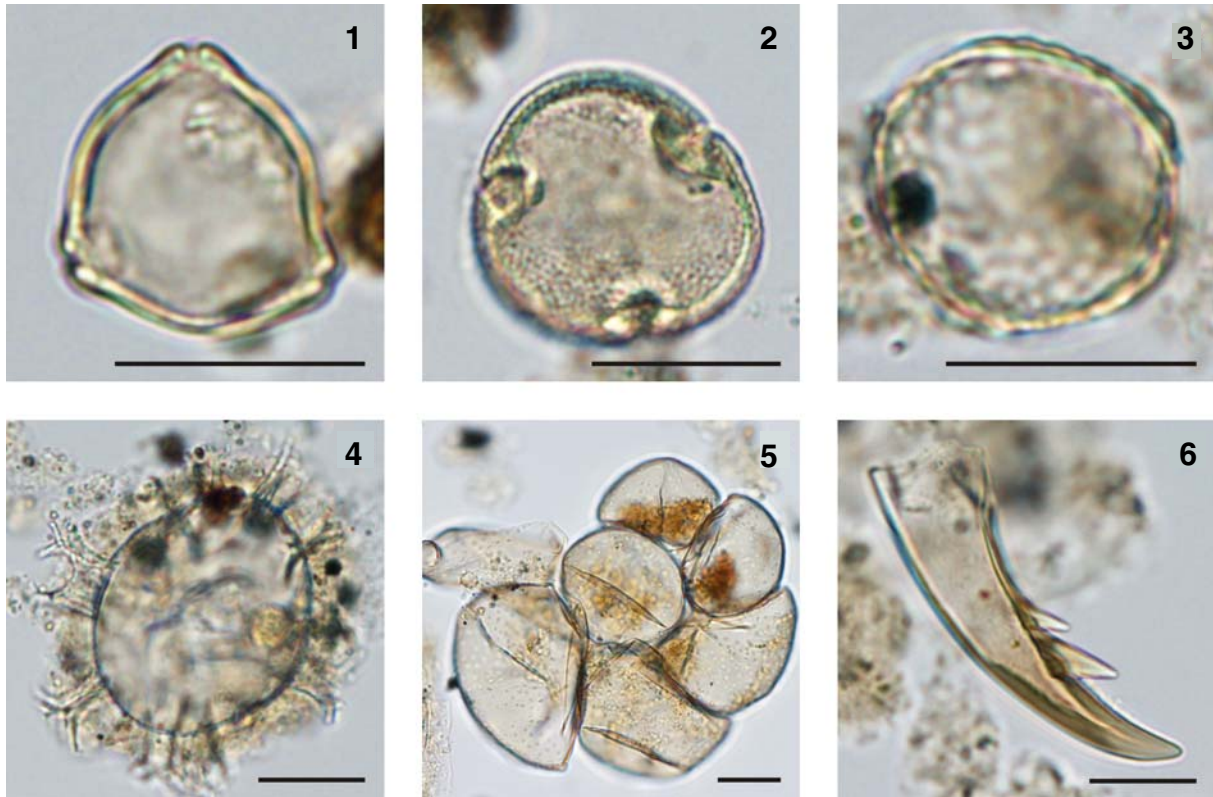


Figure F6. Pollen diagram with bisaccate pollen included in the reference sum, Core 351-M0067A-1H. For all samples included in the diagram, >100 pollen grains have been counted.

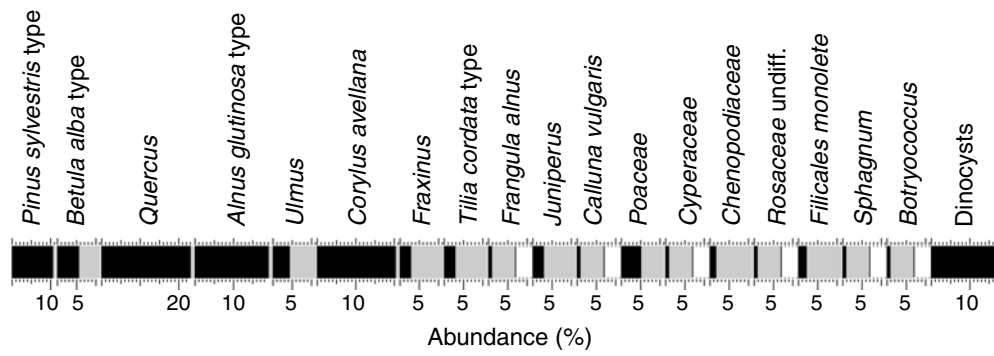




Figure F7. Concentrations of (A) chloride, (B) salinity calculated from refractive index, (C) chloride-based salinity, and (D) alkalinity in interstitial water samples, Site M0067.

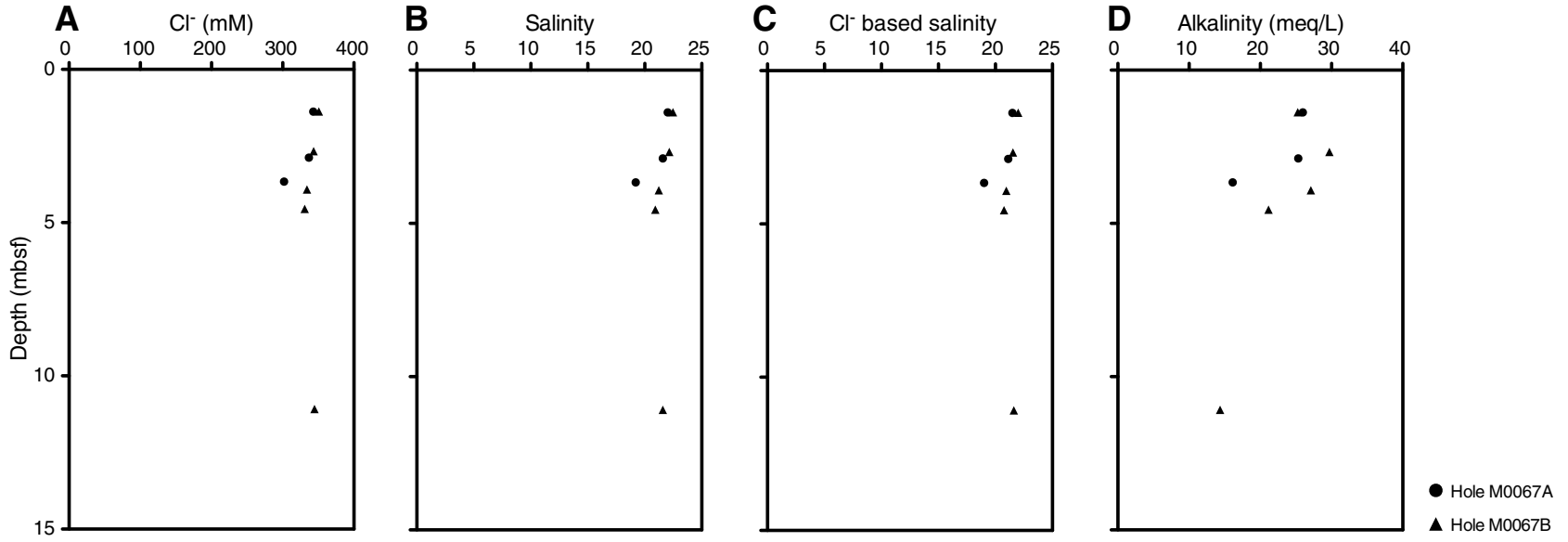




Figure F8. Concentrations and ratios of (A) sulfate, (B) sulfate/chloride, (C) hydrogen sulfide, (D) iron, (E) manganese, (F) ammonium, (G) phosphate, and (H) pH from interstitial water samples, Site M0067. Dashed line = seawater ratio.

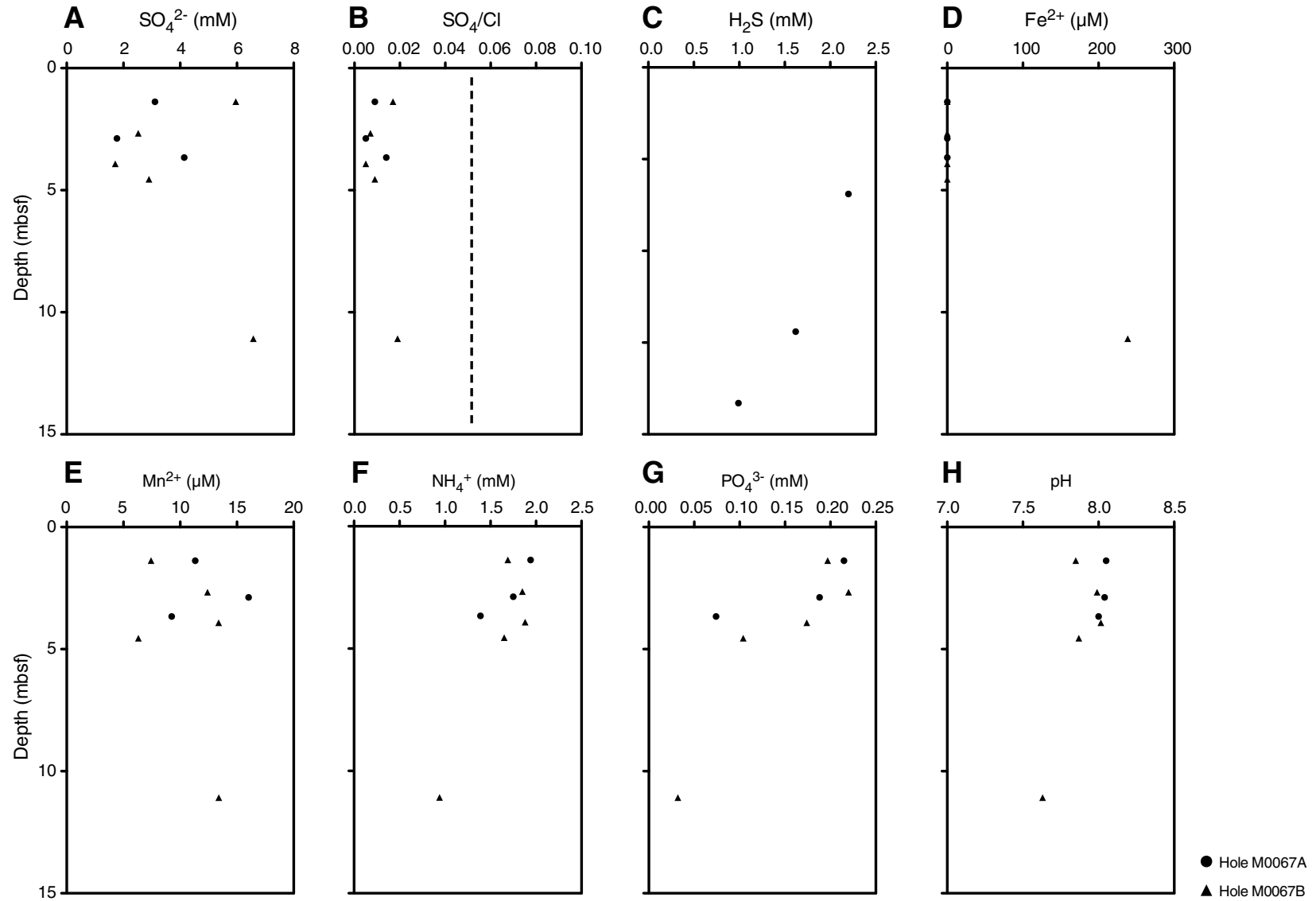




Figure F9. Concentrations and ratios of (A) bromide, (B) bromide/chloride, (C) boron, and (D) boron/chloride from interstitial water samples at Site M0067. Dashed lines = seawater ratio.

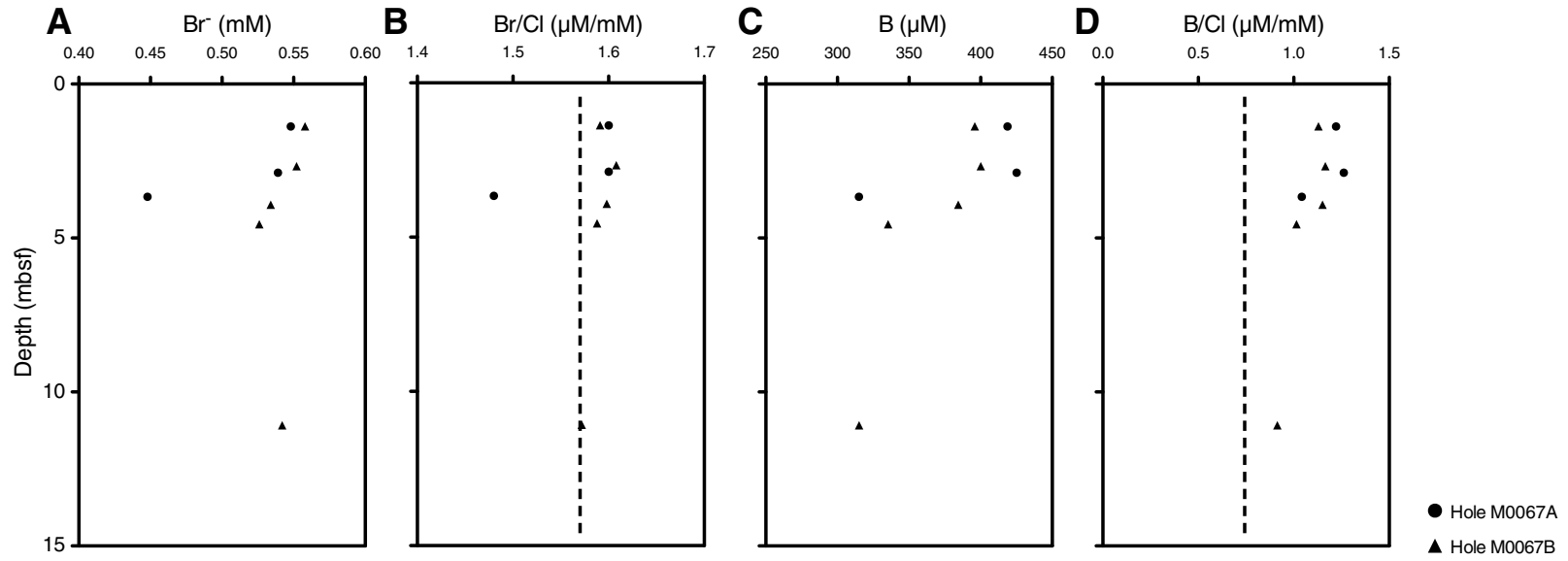




Figure F10. Concentrations and ratios of (A) sodium, (B) potassium, (C) magnesium, (D) calcium, (E) sodium/chloride, (F) potassium/chloride, (G) magnesium/chloride, and (H) calcium/chloride from interstitial water samples, Site M0067. Dashed lines = seawater ratio.

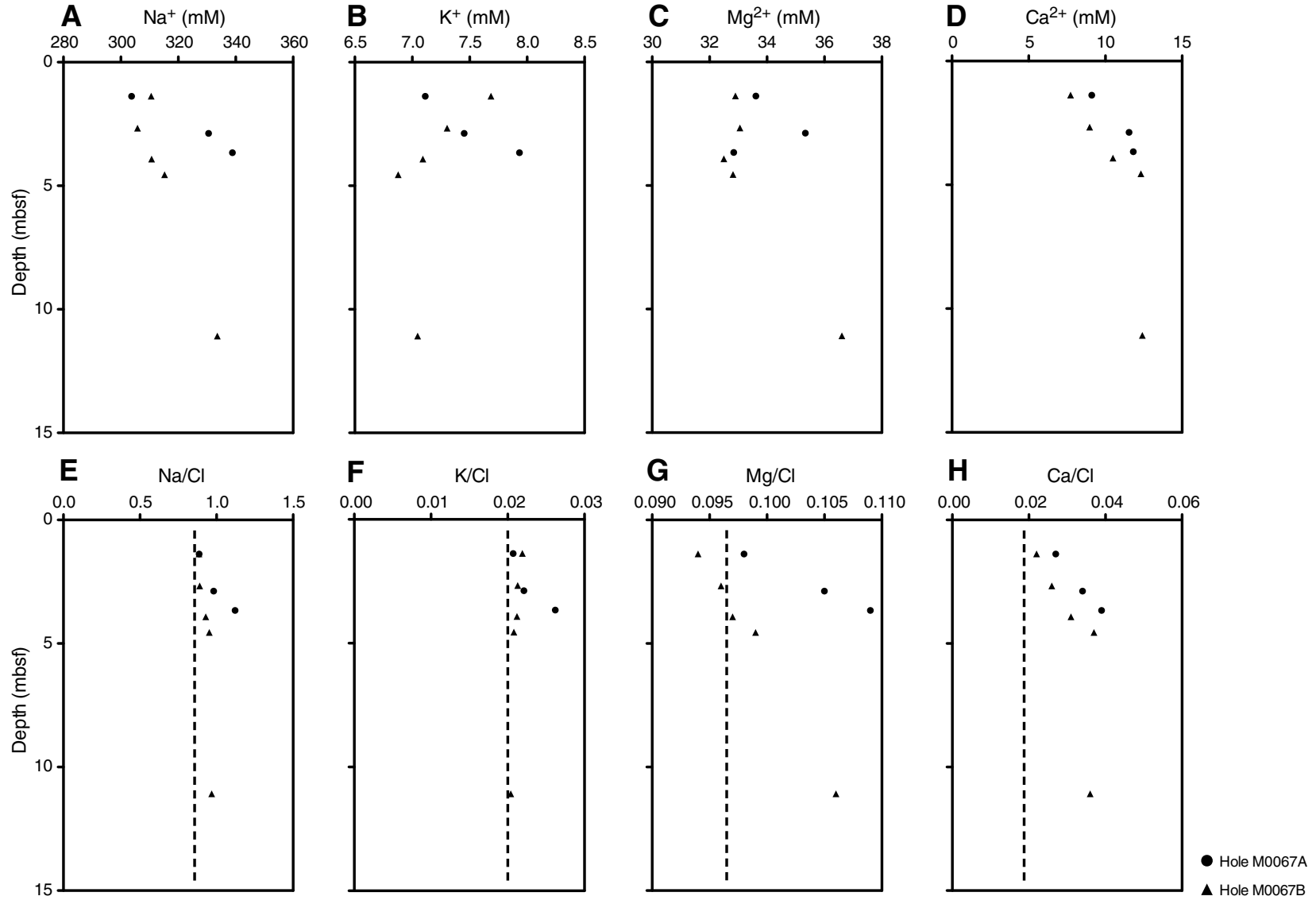




Figure F11. Concentrations of (A) strontium, (B) lithium, (C) silica, and (D) barium from interstitial water samples, Site M0067.

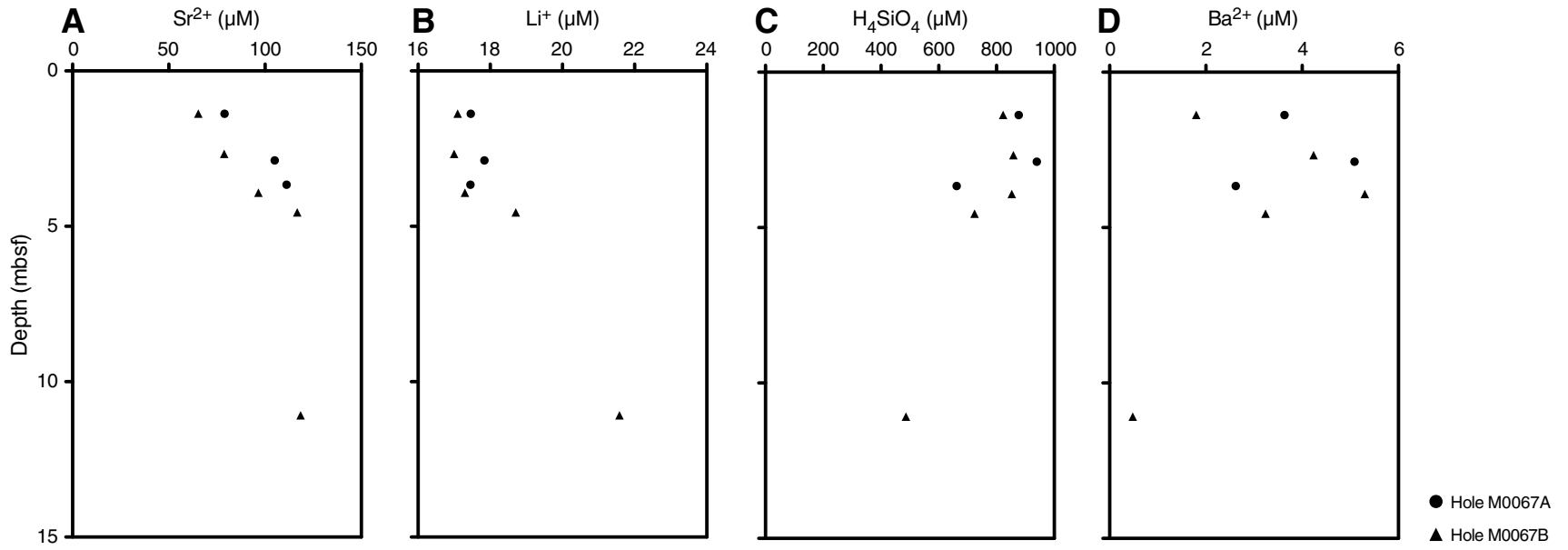




Figure F12. Sedimentary (A) total carbon (TC), (B) total organic carbon (TOC), (C) total inorganic carbon (TIC), and (D) total sulfur (TS) values, Site M0067.

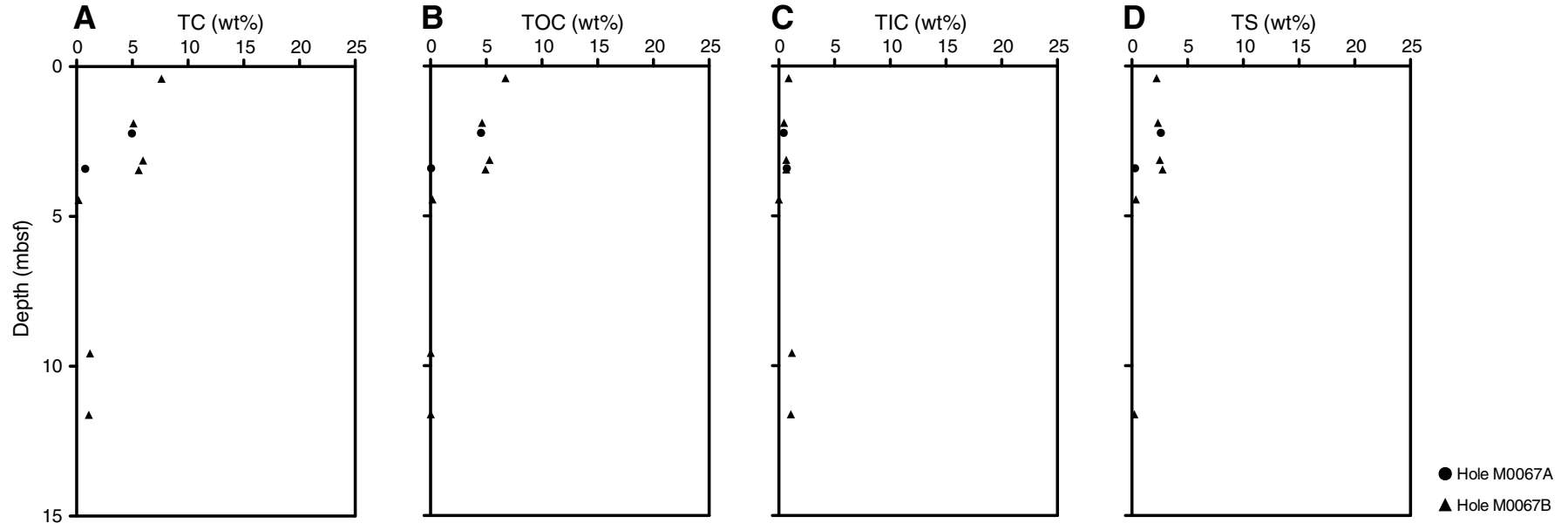


Figure F13. Natural gamma radiation (NGR) (cps), magnetic susceptibility (MS) (10^{-5} MS), noncontact resistivity (NCR) (Ωm), and dry density (g/cm^3), Hole M0067B. Depths shown for data from 9.7 mbsf to the bottom of the hole should be treated with caution as recovery from Core 347-M0067B-5H was recorded as >250%, pushing apparent depths beyond the official base of the hole at 10.9 mbsf.

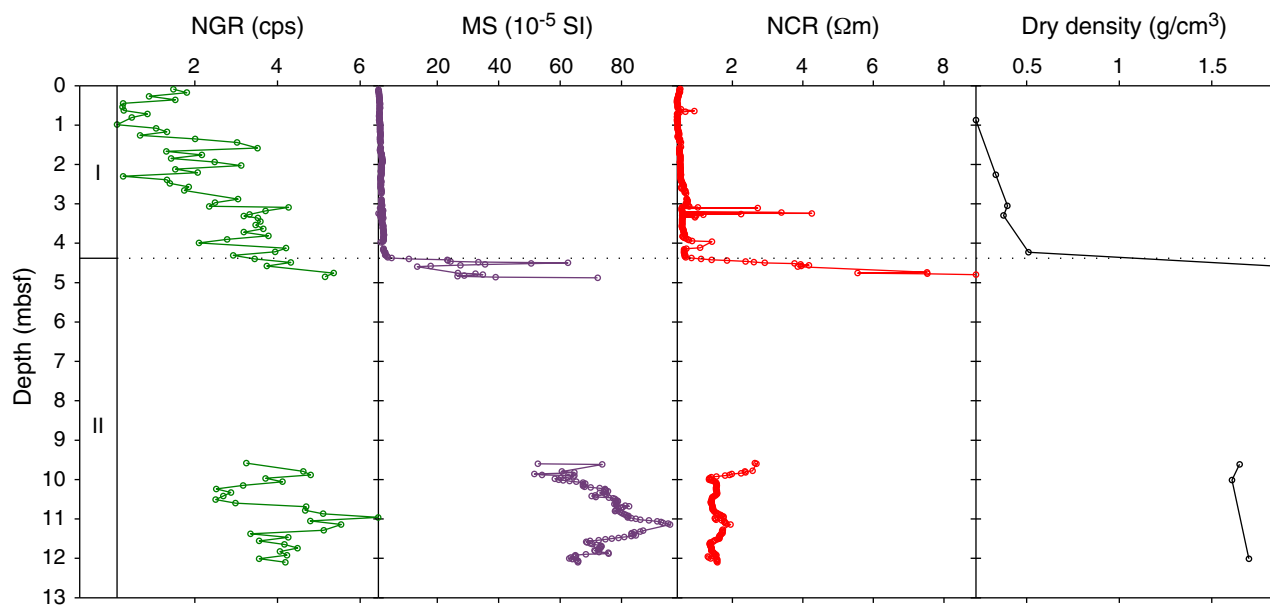




Figure F14. Plots and biplots of magnetic susceptibility (χ), natural remanent magnetization (NRM) intensity, and NRM inclination of discrete paleomagnetic samples, Holes M0067A and M0067B. Dashed line = geocentric axial dipole (GAD) prediction of inclination for the site latitude. AF = alternating field.

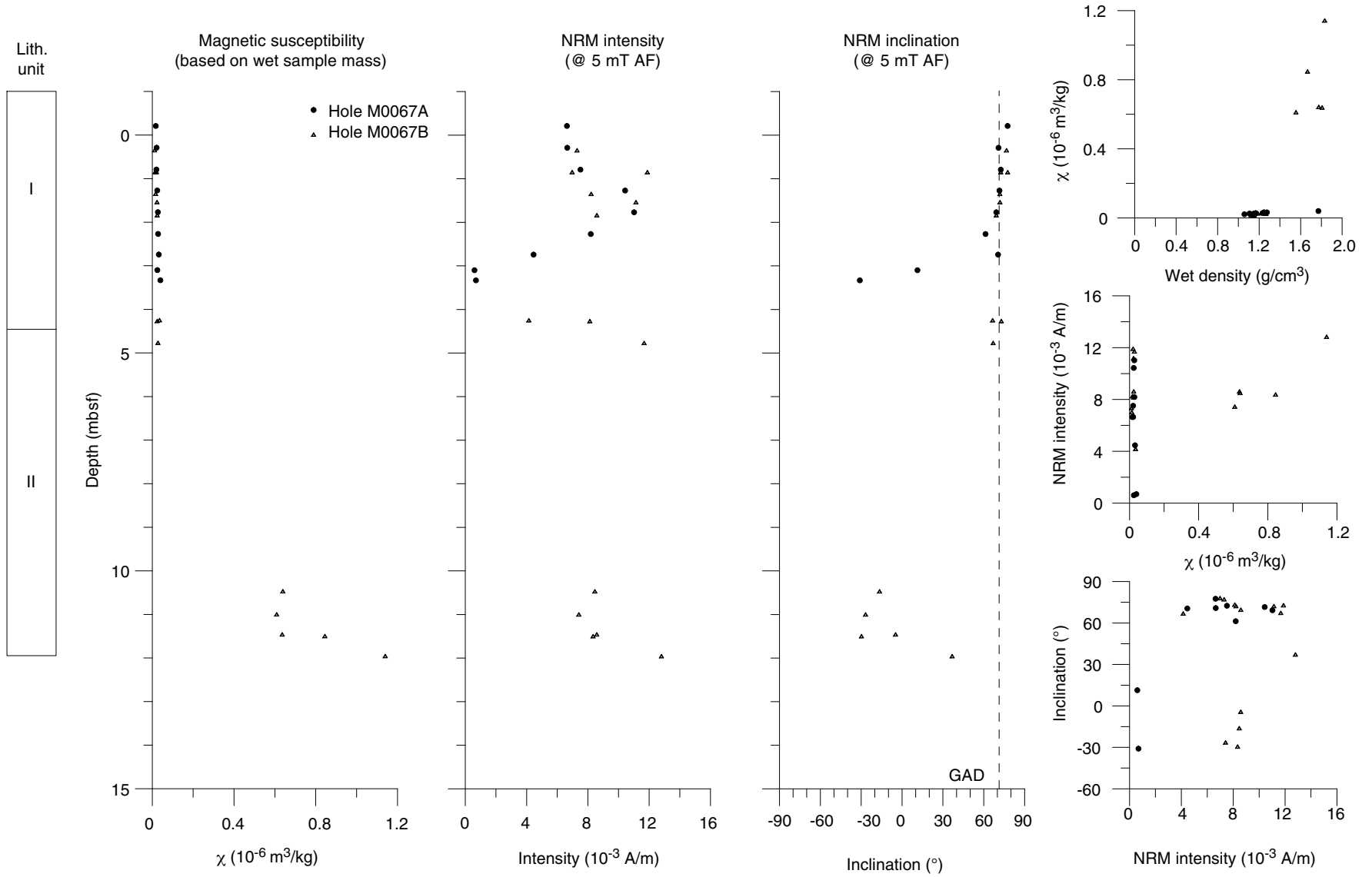


Figure F15. Plots of natural remanent magnetization (NRM) after alternating field (AF) demagnetization to 80 mT **A.** Sample 347-M0067B-2H-1, 73 cm; 4.75 mbsf. **B.** Sample 347-M0067B-5H-1, 130 cm; 10.01 mbsf. Category 1 includes samples that are not magnetically stable. Category 2 contains a vector that trends toward the origin during demagnetization and shows a higher magnetic stability than the Category 1 sample. Open squares = vertical, solid squares = horizontal.

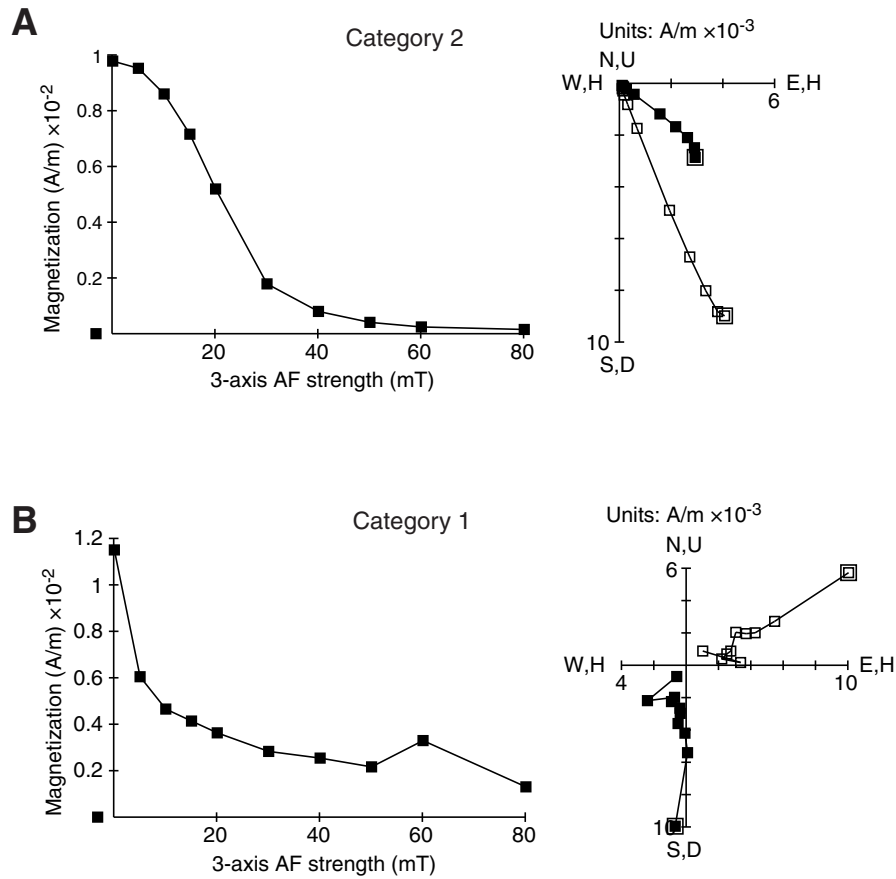


Figure F16. Plot of magnetic susceptibility data, Hole M0067A.

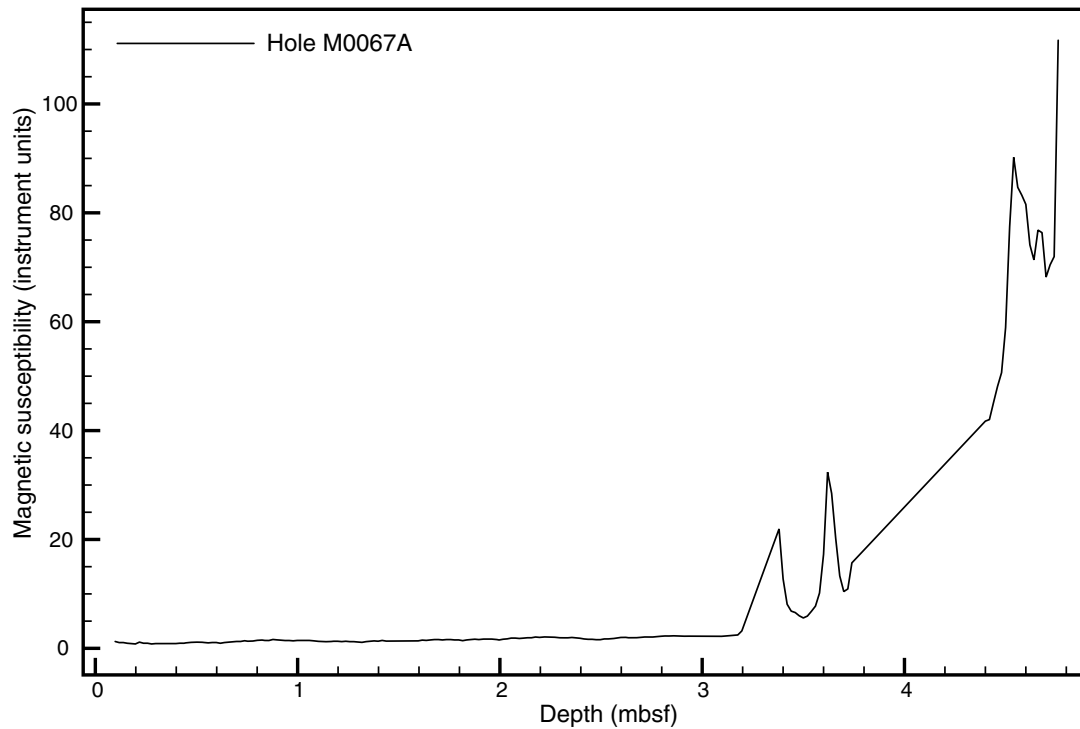


Figure F17. Correlation of seismic profile with lithostratigraphic boundaries, Site M0067. Seismic Units I, II, and III are shown in figure. Seismic Unit I corresponds to lithostratigraphic Unit I, and Seismic Units II and III correspond to lithostratigraphic Unit II. Red line indicates the proposed original site, green line indicates drilled Site M0067. SF = seafloor.

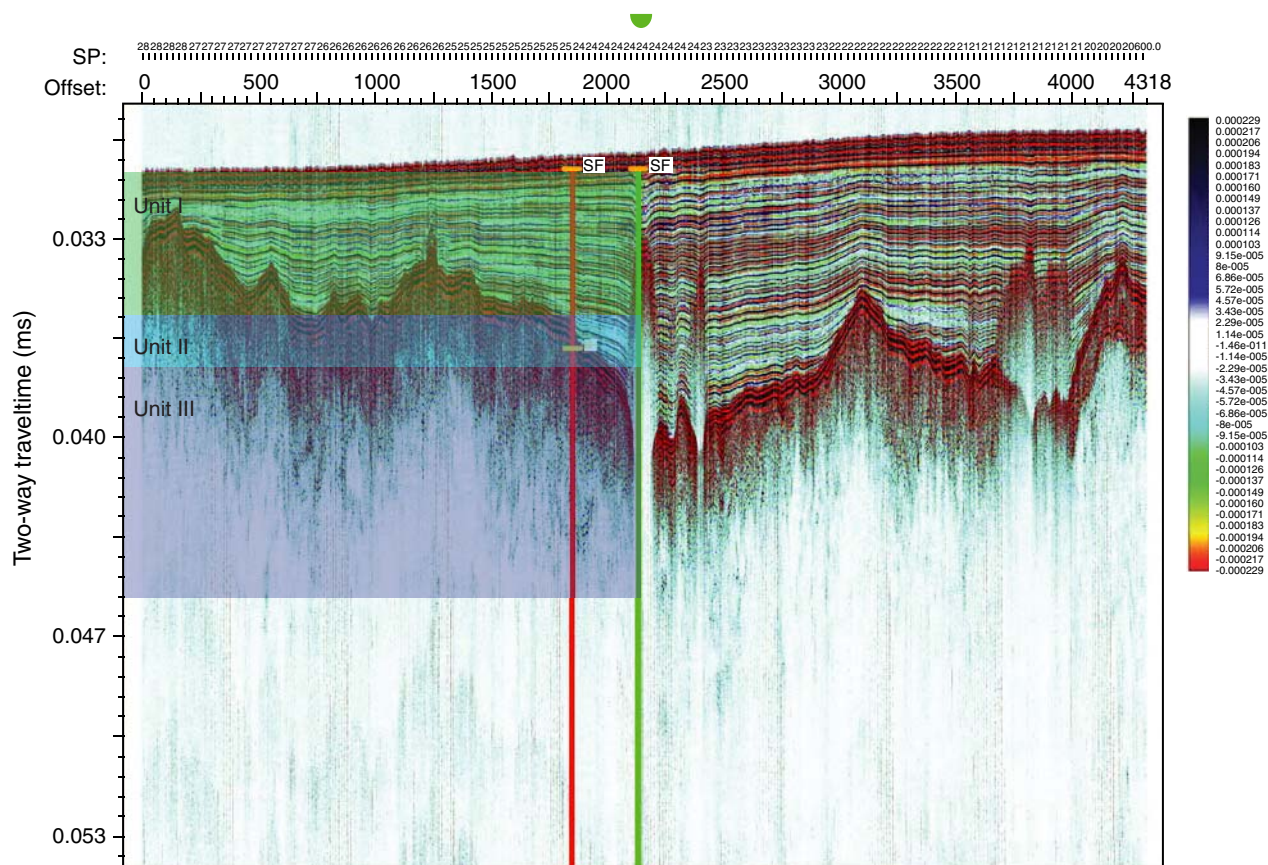




Table T1. Operations, Site M0067.

Core	Coring method	Date (2013)	Time (UTC)	Depth (mbsf)		Recovered (m)	Recovery (%)	Mud type	Comments
				Top	Bottom				
347-M0067A-									
		28 Oct	0830						On location
		28 Oct	0845						Bit guide on seabed frame in moonpool; ready to lower frame to seabed
		28 Oct	0852						Seabed frame on seabed
		28 Oct	0909						BHA on string (core barrel + 2 collars)
		28 Oct	0926						PCS in mousehole
1H	PCS	28 Oct	0935	0.00	3.30	3.29	99.7	Seawater	50 bar and down to zero
2H	PCS	28 Oct	0955	3.30	4.30	0.53	53	Seawater	70 bar, then up to 120 bar, down to 60 bar and stayed there; not full stroke; possible sand
3H	PCS	28 Oct	1025	4.30	5.30	0.57	57	Guar	
4H	PCS	28 Oct	1050	5.30	6.30	0.05	5	Guar	
5H	PCS	28 Oct	1125	6.30	7.30	0.20	20	Guar	
6H	PCS	28 Oct	1145	7.30	8.30	0.30	30	Guar	
7H	PCS	28 Oct	1210	8.30	9.30	0.30	30	Guar	
		28 Oct	1245	9.30					Attempted to wash down to 12 mbsf to take HS; driller noted change in drilling parameters and stopped at a depth calculated to be 9.3 mbsf; a roughneck was detailed to the rooster box, but before he got halfway he was recalled, as the wind had suddenly picked up to a strong level; (60kt) within a very short time (seconds) the ship then moved, apparently bending the string; driller was able to trip one pipe off the string and sky the remainder to make the string safe; template was brought back on deck and the drill deck made secure
347-M0067B-									
		28 Oct	2040						On location; waited on weather and built differential GPS model
		28 Oct	2140						Ran pipe
1H	PCS	28 Oct	2205	0.00	3.00	3.44	114.67	Seawater	Fired 1 m above calculated seabed from Hole M0067A to gain overlap
2H	PCS	28 Oct	2235	3.00	5.00	1.96	98	Seawater	
3O	NCA	28 Oct	2330	5.00	9.50	0.00	0	Guar	Open hole to level where day shift driller noted a change in parameters before winds increased
4H	PCS	28 Oct	2337	9.50	9.70	0.15	75	Guar	Sand and gravel
5H	PCS	28 Oct	2358	9.70	10.70	2.52	252	Guar	Sand with some gravel
6S	HS	29 Oct	0020	10.70	10.90	0.10	50	Guar	
		29 Oct	0040						End of hole
		29 Oct	0105						Tripped pipe Seabed frame on deck

HS = hammer sampler, NCA = noncoring assembly, PCS = piston coring system. BHA = bottom-hole assembly.

Table T2. Diatom species, Site M0067.

Taxonomic list	Taxonomic list
<p>Marine taxa</p> <p><i>Actinoptychus senarius</i> (Ehrenberg) Ehrenberg</p> <p><i>Amphora crassa</i> Gregory</p> <p><i>Ardissonea fulgens</i> (Greville) Grunow</p> <p><i>Caloneis elongata</i> (Grunow) Boyer</p> <p><i>Dimeregramma minor</i> (Gregory) Ralfs</p> <p><i>Diploneis coffaeiformis</i> (Schmidt) Cleve</p> <p><i>Diploneis subcincta</i> (A. Schmidt) Cleve</p> <p><i>Eucampia zodiacus</i> Ehrenberg</p> <p><i>Fallacia litoricola</i> (Hustedt) D.G. Mann</p> <p><i>Hyalodiscus scoticus</i> (Kützing) Grunow</p> <p><i>Licmophora abbreviata</i> C. Agardh</p> <p><i>Lyrella</i> cf. <i>spectabilis</i> (Gregory) D.G. Mann</p> <p><i>Navicula ramosissima</i> (C. Agardh) Cleve</p> <p><i>Nitzschia marginulata</i> Grunow</p> <p><i>Nitzschia scabra</i> Cleve</p> <p><i>Odontella aurita</i> (Lyngbye) C. Agardh</p> <p><i>Opephora marina</i> (Gregory) Petit</p> <p><i>Opephora pacifica</i> (Grunow) Petit</p> <p><i>Pinnularia quadratarea</i> (A. Schmidt) Cleve</p> <p><i>Plagiogramma staurophorum</i> (W. Gregory) Heiberg</p> <p><i>Pleurosigma angulatum</i> (Queckett) W. Smith</p> <p><i>Porosira glacialis</i> (Grunow) Jorgensen</p> <p><i>Pseudosolenia calcar-avis</i> (Schultze) B.G. Sundström</p> <p><i>Thalassiosira eccentrica</i> (Ehrenberg) Cleve</p> <p><i>Toxarium undulatum</i> Bailey</p> <p><i>Trachyneis aspera</i> (Ehrenberg) Cleve</p> <p><i>Thalassiosira oestrupii</i> (Ostenfeld) Hasle</p> <p>Brackish-marine taxa</p> <p><i>Achnanthes brevipes</i> var. <i>intermedia</i> (Kützing) Cleve</p> <p><i>Achnanthes longipes</i> Agardh</p> <p><i>Actinocyclus octonarius</i> Ehrenberg</p> <p><i>Bacillaria socialis</i> (Gregory) Ralfs</p> <p><i>Caloneis crassa</i> (Gregory) R. Ross</p> <p><i>Chaetoceros</i> spp. vegetative cells</p> <p><i>Chaetoceros</i> spp. resting spores</p> <p><i>Cocconeis peltooides</i> Hustedt</p> <p><i>Cocconeis stauroneiformis</i> (W. Smith) Okuno</p> <p><i>Grammatophora macilenta</i> W. Smith</p> <p><i>Grammatophora oceanica</i> Ehrenberg</p> <p><i>Mastogloia exigua</i> F.W. Lewis</p> <p><i>Petroneis granulata</i> (Bailey) Mann</p> <p><i>Rhabdonema arcuatum</i> (Lyngbye) Kützing</p> <p><i>Rhopalodia acuminata</i> Krammer</p> <p><i>Tabularia fasciculata</i> (C. Agardh) D.M. Williams and Round</p> <p><i>Thalassionema nitzschioides</i> (Grunow) Mereschkowsky</p> <p><i>Tryblionella coarctata</i> (Grunow) D.G. Mann</p> <p>Brackish taxa</p> <p><i>Amphora robusta</i> Gregory</p> <p><i>Amphora subholstatica</i> Krammer</p> <p><i>Brachysira aponina</i> Kützing</p>	<p><i>Caloneis aemula</i> (A. Schmidt) Cleve</p> <p><i>Caloneis amphisbaena</i> (Bory) Cleve</p> <p><i>Cocconeis placentula</i> var. <i>euglypta</i> (Ehrenberg) Grunow</p> <p><i>Cocconeis scutellum</i> Ehrenberg</p> <p><i>Coscinodiscus granii</i> Gough</p> <p><i>Cyclotella choctawhatcheeana</i> Prasad</p> <p><i>Cyclotella striata</i> (Kützing) Grunow</p> <p><i>Diploneis didyma</i> (Ehrenberg) Ehrenberg</p> <p><i>Diploneis domblittensis</i> (Grunow) Cleve</p> <p><i>Diploneis interrupta</i> (Kützing) Cleve</p> <p><i>Diploneis stroemii</i> Hustedt</p> <p><i>Epithemia adnata</i> (Kützing) Brébisson</p> <p><i>Mastogloia pusilla</i> Grunow</p> <p><i>Navicula digitoradiata</i> (Gregory) Ralfs</p> <p><i>Navicula palpebralis</i> Brébisson ex W. Smith</p> <p><i>Navicula peregrina</i> (Ehrenberg) Kützing</p> <p><i>Opephora mutabilis</i> (Grunow) Sabbe and Wyverman</p> <p><i>Paralia sulcata</i> (Ehrenberg) Cleve</p> <p><i>Parlibellus plicatus</i> (Donkin) Cox</p> <p><i>Planothidium quarnerensis</i> (Grunow) Witkowski, Lange</p> <p><i>Rhoicosphenia curvata</i> (Kützing) Grunow</p> <p><i>Skeletonema costatum</i> (Greville) Cleve</p> <p><i>Thalassiosira levanderi</i> Van Goor</p> <p><i>Thalassiosira proschkinae</i> Makarova</p> <p>Brackish-freshwater taxa</p> <p><i>Actinocyclus octonarius</i> var. <i>crassus</i> (W. Smith) Hendey</p> <p><i>Amphora ovalis</i> (Kützing) Kützing</p> <p><i>Amphora pediculus</i> (Kützing) Grunow ex A. Schmidt</p> <p><i>Campylodiscus bicostatus</i> W. Smith</p> <p><i>Cocconeis pediculus</i> Ehrenberg</p> <p><i>Diploneis smithii</i> (Brébisson) Cleve</p> <p><i>Epithemia turgida</i> var. <i>westermanni</i> (Ehrenberg) Grunow</p> <p><i>Gyrosigma acuminatum</i> (Kützing) Rabenhorst</p> <p><i>Nitzschia heufferiana</i> Grunow</p> <p><i>Pinnularia accuminata</i> (Smith)</p> <p><i>Rhopalodia gibba</i> (Ehrenberg) O. Müller</p> <p><i>Thalassiosira baltica</i> (Grunow) Ostenfeld</p> <p>Freshwater taxa</p> <p><i>Aneumastus tusculus</i> (Ehrenberg) D.G. Mann and A.J. Stickle</p> <p><i>Aulacoseira granulata</i> (Ehrenberg) Simonsen</p> <p><i>Diploneis mauleri</i> (Brun) Cleve</p> <p><i>Diploneis parma</i> Cleve</p> <p>Uncertain affinity</p> <p><i>Cerataulus turgidus</i> (Ehrenberg) Ehrenberg</p> <p>Salinity affinities follows Snoeijns et al. (1993–1998). Diatom authorities according to AlgaeBase (www.algaebase.org).</p>



Table T3. Diatoms, Hole M0067B. (Continued on next page.)

Affinity	Life form	Diatoms	Depth (mbsf):								
			Core, section, interval (cm):		0	1.49	2.79	3	4.095	9.7	11.2
			1H-1	1H-2	1H-3	2H-1	2H-2, 4-5	5H-1	5H-2	Barren	2 valves
BM		<i>Achnanthes brevipes</i> var. <i>intermedia</i> (Kützing) Cleve			x						
BM	Pelagic	<i>Actinocyclus octonarius</i> Ehrenberg				x	x				
BF	Pelagic	<i>Actinocyclus octonarius</i> var. <i>crassus</i> (W. Smith) Hendey						x			
M	Benthic	<i>Actinoptychus senarius</i> (Ehrenberg) Ehrenberg	x	x	x	x	x				
M		<i>Amphora crassa</i> Gregory									x
BF	Epipellic and epilithic	<i>Amphora ovalis</i> (Kützing) Kützing	x	x		x	x				
BF	Epipellic and epilithic	<i>Amphora pediculus</i> (Kützing) Grunow ex A. Schmidt	x			x					
B	Epipellic	<i>Amphora robusta</i> Gregory	x	x	x						
B	Epipellic and epiphytic	<i>Amphora subholstatica</i> Krammer				x					
F	Epipellic	<i>Aneumastus tusculus</i> (Ehrenberg) D.G. Mann and A.J. Stickle		x							
M	Epiphytic	<i>Ardissonea fulgens</i> (Greville) Grunow		x	x	x					
BM	Epipellic and epilithic	<i>Bacillaria socialis</i> (Gregory) Ralfs		x		x					
B		<i>Brachysira aponina</i> Kützing				x					
B	Epipellic	<i>Caloneis amphisbaena</i> (Bory) Cleve	x								
BM	Epipellic	<i>Caloneis crassa</i> (Gregory) R. Ross						x			
M	Epipellic?	<i>Caloneis elongata</i> (Grunow) Boyer		x		x					
BF	Epipellic	<i>Campylodiscus bicostatus</i> W. Smith	x		x						
?	?	<i>Cerataulus turgidus</i> (Ehrenberg) Ehrenberg	x								
BM	Pelagic	<i>Chaetoceros</i> resting spores spp.	x	x	x	x	x				
BF	Epiphytic	<i>Cocconeis pediculus</i> Ehrenberg				x					
BM	Epipsammic	<i>Cocconeis peltoides</i> Hustedt	x	x							
B	Epiphytic and episammic	<i>Cocconeis placentula</i> var. <i>euglypta</i> (Ehrenberg) Grunow				x					
B	Epiphytic	<i>Cocconeis scutellum</i> Ehrenberg	x	x	x	x	x				
BM	Epiphytic	<i>Cocconeis stauroneiformis</i> (W. Smith) Okuno						x			
B	Pelagic	<i>Coccinodiscus granii</i> Gough			x						
B	Pelagic and epilithic	<i>Cyclotella choctawhatcheeana</i> Prasad	x								
B	Littoral?	<i>Cyclotella striata</i> (Kützing) Grunow						x			
M	Benthic	<i>Dimeregramma minor</i> (Gregory) Ralfs	x	x	x	x	x				
M	Epipellic?	<i>Diploneis coffaeiformis</i> (Schmidt) Cleve						x			
B	Epipellic	<i>Diploneis didyma</i> (Ehrenberg) Ehrenberg	x	x	x	x	x				
B	Epipellic	<i>Diploneis domblittensis</i> (Grunow) Cleve			x						
B	Epipellic	<i>Diploneis interrupta</i> (Kützing) Cleve				x					
BF	Epipellic	<i>Diploneis smithii</i> (Brébisson) Cleve	x	x	x	x	x				
B	Epipellic	<i>Diploneis stroemii</i> Hustedt						x			
M	Epipellic?	<i>Diploneis subcineta</i> (A. Schmidt) Cleve						x			
B	Epiphytic	<i>Epithemia adnata</i> (Kützing) Brébisson		x	x						
M		<i>Fallacia litoricola</i> (Hustedt) D.G. Mann	x								
BM		<i>Grammatophora macilenta</i> W. Smith				x					
BM	Epiphytic	<i>Grammatophora oceanica</i> Ehrenberg	x	x	x	x					
M	Epiphytic	<i>Hyalodiscus scoticus</i> (Kützing) Grunow	x	x	x	x	x				
M	Epiphytic	<i>Licmophora abbreviata</i> C. Agardh				x					
M		<i>Lyrella</i> cf. <i>spectabilis</i> (Gregory) D.G. Mann			x	x					
BM	Epipellic and epilithic	<i>Mastogloia exigua</i> F.W. Lewis	x	x	x	x					
B	Epipellic and epilithic	<i>Mastogloia pusilla</i> Grunow		x		x					x
B		<i>Navicula digitoradiata</i> (Gregory) Ralfs	x		x	x	x				
B		<i>Navicula palpebralis</i> Brébisson ex W. Smith		x							
M		<i>Navicula ramosissima</i> (C. Agardh) Cleve	x		x	x					
M		<i>Nitzschia marginulata</i> Grunow		x							
M	Sea ice	<i>Nitzschia scabra</i> Cleve				x					



Table T3 (continued).

Affinity	Life form	Diatoms	Depth (mbsf):								
			0	1.49	2.79	3	4.095	9.7	11.2		
			Core, section, interval (cm):								
			1H-1	1H-2	1H-3	2H-1	2H-2, 4-5	5H-1	5H-2		
										Barren	2 valves
M	Epiphytic and epipelagic	<i>Odontella aurita</i> (Lyngbye) C. Agardh	x	x	x	x					
M	Epipsammic	<i>Opephora marina</i> (Gregory) Petit		x		x		x			
B	Epipsammic and epiphytic	<i>Opephora mutabilis</i> (Grunow) Sabbe and Wyverman	x			x					
M		<i>Opephora pacifica</i> (Grunow) Petit	x		x	x					
B	Tycho planktonic	<i>Paralia sulcata</i> (Ehrenberg) Cleve	x	x	x	x		c			
B	Epipelagic	<i>Parlibellus plicatus</i> (Donkin) Cox				x					
BF	Epipelagic	<i>Pinnularia accuminata</i> (Smith)			x	x					
M		<i>Pinnularia quadratarea</i> (A. Schmidt) Cleve	x								
M	Benthic	<i>Plagiogramma stauraphorum</i> (W. Gregory) Heiberg	x	x	x	x		x			
B	Epipsammic?	<i>Planothidium quarnerensis</i> (Grunow) Witkowski, Lange-Bertalot and Metzelin	x	x							
M	Epipelagic	<i>Pleurosigma angulatum</i> (Queckett) W. Smith	x	x	x	x					
M	Pelagic	<i>Porosira glacialis</i> (Grunow) Jorgensen	x	x	x						
M	Pelagic	<i>Pseudosolenia calcar-avis</i> (Schultze) B.G. Sundström	x	x		x		x			
BM	Epiphytic and epilithic	<i>Rhabdonema arcuatum</i> (Lyngbye) Kützing	x	x	x			x			
B	Epiphytic and epilithic	<i>Rhoicosphenia curvata</i> (Kützing) Grunow	x	x	x						
BM	Epipelagic and epilithic	<i>Rhopalodia acuminata</i> Krammer	x	x	x	x		x			
BF	Epipelagic and epilithic	<i>Rhopalodia gibba</i> (Ehrenberg) O. Müller	x	x	x	x					
B	Pelagic	<i>Skeletonema costatum</i> (Greville) Cleve		x		x					
BM	Epiphytic	<i>Tabularia fasciculata</i> (C. Agardh) D.M. Williams and Round	x	x	x	x		x			
BM	Pelagic	<i>Thalassionema nitzschioides</i> (Grunow) Mereschkowsky	x	x	x	x		x			
BF	Pelagic	<i>Thalassiosira baltica</i> (Grunow) Ostefeld	x	x		x					
M	Pelagic	<i>Thalassiosira eccentrica</i> (Ehrenberg) Cleve	x	x	x	x					
B	Pelagic	<i>Thalassiosira levanderi</i> Van Goor	x	x							
M?	Pelagic	<i>Thalassiosira oestrupii</i> (Ostefeld) Hasle	x	x		x		x			
B	Pelagic	<i>Thalassiosira proschkinae</i> Makarova			x	x					
M	?	<i>Toxarium undulatum</i> Bailey	x		x	x		x			
M	Epipelagic	<i>Trachyneis aspera</i> (Ehrenberg) Cleve	x	x	x			x			
BM	Epipelagic	<i>Tryblionella coarctata</i> (Grunow) D.G. Mann		x	x			x			
		<i>Dictyocha speculum</i>	x	x	x	x		x			
		Chrysophyte cysts									
		Short ridges						x			

F = freshwater, BF = brackish-freshwater, B = brackish, BM = brackish-marine, M = marine.

Table T4. Foraminifers, Site M0067.

Hole, core, section, interval (cm)	Depth (mbsf)		Abundance	Number of species	Agglutinated (all species)	<i>Ammonia beccarii</i>	<i>Elphidium albiumbilicatum</i>	<i>Elphidium excavatum clavatum</i>	<i>Elphidium excavatum selseyensis</i>	<i>Elphidium incertum</i>	<i>Elphidium williamsoni</i>	Other <i>Elphidium</i> and <i>Haymesina</i> spp.	<i>Quinqueloculina</i> sp.	<i>Stainforthia feylingia</i>
	Top	Bottom												
347-														
M0067A-1H-1, 15-17	0.15	0.17	C	4	x	x		x	x					
M0067B-1H-1, 20-22	0.20	0.22	C	2	x	x								
M0067A-1H-1, 75-77	0.75	0.77	A	4	x	x				x		x		
M0067B-1H-1, 75-77	0.75	0.77	R	2	x					x		x		
M0067B-1H-2, 15-17	1.64	1.66	A	1	x									
M0067A-1H-2, 15-17	1.65	1.67	A	3	x		x							x
M0067A-1H-CC	3.23	3.25	A	4	x	x	x					x		
M0067A-1H-CC	3.25	3.29	C	3		x	x					x		
M0067B-1H-CC	3.16	3.44	C	2	x							x		
M0067A-2H-1, 21-23	3.51	3.53	R	6	x	x		x		x	x	x		
M0067A-2H-CC	3.78	3.83	B											
M0067B-2H-2, 12-14	4.16	4.18	A	9	x	x	x	x	x	x	x	x	x	
M0067A-3H-CC	4.80	4.87	B											
M0067B-2H-CC	4.94	4.96	B											
M0067A-4H-CC	5.30	5.35	B											
M0067A-5H-CC	6.30	6.50	B											
M0067A-6H-CC	7.30	7.60	B											
M0067A-7H-CC	8.30	8.60	B											
M0067B-6S	10.75	10.80	B											
M0067B-5H-2, 15-17	11.35	11.37	B											
M0067B-5H-CC	12.17	12.22	B											

Abundance: A = abundant, C = common, R = rare, B = barren.

Table T5. Distribution and abundance of ostracods, Site M0067.

Core, section, interval (cm)	Depth (mbsf)	Overall abundance/20 cm ³ Abundance (offshore samples, 5–30 cm ³)	<i>Acanthocythereis dunelmensis</i>	<i>Cytheropteron latissimum</i>	<i>Eolisonella concinna</i>	<i>Finmarchinella</i> sp.	<i>Robertsonites tuberculatus</i>	<i>Sarsicytheridea bradii</i>	<i>Sarsicytheridea punctillata</i>	Undetermined
347-M0067A-										
1H-1, 15–17	0.16	B								
1H-1, 75–77	0.76	R								R
1H-2, 15–17	1.66	B								
1H-CC, 0–6	3.23	A	R	R	C	R	F	C	C	R
1H-CC, 0–5	3.25	F		R	R			F	F	R
2H-1, 21–23	3.52	A			C		R	F	F	
2H-CC, 0–7	3.78	B								
3H-CC, 0–5	4.8	B								
4H-CC, 0–20	5.3	B								
5H-CC, 0–30	6.3	B								
6H-CC, 0–30	7.3	B								
7H-CC	8.3	B								
347-M0067B-										
1H-1, 20–22	0.21	R								R
1H-1, 75–77	0.76	B								
1H-2, 15–17	1.65	B								
1H-CC, 28–28	3.44	B								
2H-2, 12–14	4.17	F					R	R		
2H-CC, 24–29	4.91	B								
6S-CC, 5–10	10.75	B								
5H-2, 15–17	11.36	B								
5H-CC, 0–5	12.17	B								

Abundance: A = abundance, C = common, F = few, R = rare, B = barren.

Table T6. Interstitial water geochemistry, Site M0067.

Core, section, interval (cm)	Type	Depth (mbsf)	Volume (mL)	Analyte:	pH	Salinity	Alkalinity	Cl ⁻	Br ⁻	SO ₄ ²⁻	H ₂ S	NH ₄ ⁺	Na ⁺	K ⁺	Mg ²⁺	Ca ²⁺	Sr ²⁺	Li ⁺	H ₄ SiO ₄	Ba ²⁺	B	Al	PO ₄ ³⁻	Fe ²⁺	Mn ²⁺	Rb		
				Unit:	ISE	Refraction	meq/L	mM	mM	mM	mM	mM	mM	mM	mM	mM	mM	mM	μM	μM	μM	μM	μM	μM	μM	mM	μM	μM
				Method:			Titration	IC	IC	IC	Photometric	Conductivity	ICP-OES	ICP-OES	ICP-OES	ICP-OES	ICP-OES	ICP-OES	ICP-OES	ICP-OES	ICP-OES	ICP-OES	ICP-OES	ICP-OES	ICP-OES	ICP-OES	ICP-OES	
347-M0067A-																												
1H-1, 135-140	Rh	1.38	15		8.05	22.01	25.97	342.83	0.55	3.11	2.20	1.94	303.74	7.11	33.61	9.11	78.93	17.46	876.62	3.63	418.74	0.78	0.22	0.00	11.33	0.75		
1H-2, 135-140	Rh	2.88	15		8.04	21.59	25.34	336.79	0.54	1.77	1.62	1.75	330.54	7.45	35.33	11.54	105.03	17.84	939.29	5.09	425.12	0.33	0.19	0.00	16.02	0.78		
2H-1, 33-38	Rh	3.66	38		8.00	19.21	16.11	302.36	0.45	4.14	0.99	1.39	338.84	7.93	32.84	11.81	111.16	17.45	661.92	2.62	314.96	0.00	0.07	0.00	9.26	0.65		
347-M0067B-																												
1H-1, 134-139	Rh	1.37	31		7.85	22.47	25.26	350.77	0.56	5.96	—	1.69	310.57	7.68	32.90	7.73	65.36	17.10	822.86	1.80	395.89	0.00	0.20	0.00	7.44	0.88		
1H-2, 115-120	Rh	2.67	18		7.99	22.16	29.70	343.44	0.55	2.52	—	1.85	305.79	7.30	33.06	8.97	78.75	17.00	858.47	4.24	400.06	0.00	0.22	0.00	12.40	0.74		
2H-1, 89-94	Rh	3.92	13		8.02	21.23	27.10	334.12	0.53	1.71	—	1.88	310.70	7.09	32.50	10.50	96.54	17.30	852.77	5.30	384.42	0.00	0.17	0.00	13.39	0.69		
2H-2, 48-53	Rh	4.55	40		7.87	20.92	21.15	330.93	0.53	2.90	—	1.65	315.22	6.88	32.82	12.32	116.75	18.71	723.87	3.24	335.40	0.00	0.10	0.00	6.31	0.61		
5H-1, 135-140	Rh	11.08	40		7.63	21.59	14.36	344.61	0.54	6.58	—	0.94	333.58	7.05	36.61	12.41	118.47	21.58	486.74	0.48	315.14	0.52	0.03	238.52	13.40	0.76		
Reference samples																												
R2 salt brine mud 1	—	—	—		7.45	170.07	2.35	3448.94	0.00	17.47	0.00	0.00	3372.77	5.85	14.36	12.48	420.57	6.06	35.78	8.98	137.36	0.22	0.01	13.54	6.46	0.73		
R3 seawater from mud pump	—	—	—		7.69	16.87	2.14	265.91	0.33	11.68	0.00	0.00	254.37	4.99	23.53	5.07	45.41	11.86	7.62	3.18	187.77	0.56	0.01	0.00	2.87	0.63		
R4 grease 1 drill pipe	—	—	—		6.28	2.56	0.26	0.18	0.00	0.01	0.00	0.02	0.00	0.00	0.00	0.01	0.13	1.18	0.57	4.69	8.69	0.00	0.01	0.00	2.86	0.00		
R5 grease 2 pipes	—	—	—		6.51	3.04	0.27	0.09	0.00	0.00	0.00	0.02	0.00	0.00	0.00	0.04	0.08	0.29	0.00	4.05	6.94	0.00	0.01	0.00	2.86	0.00		
R6 grease 3 core barrel	—	—	—		6.54	4.49	0.26	0.08	0.00	0.00	0.00	0.03	0.00	0.00	0.00	0.03	0.07	0.29	1.53	3.90	6.47	0.00	0.01	0.00	2.86	0.00		
R7 grease 4 "moly" piston rod grease	—	—	—		4.34	0.00	0.11	0.05	0.00	0.00	0.00	0.00	0.00	0.00	0.00	0.00	0.01	0.41	0.00	0.43	5.09	0.00	0.01	0.00	2.86	0.00		
R8 grease 5 pipe thread	—	—	—		6.30	5.56	0.23	0.39	0.00	0.03	0.00	0.03	0.00	0.00	0.00	0.00	0.05	1.57	0.61	3.01	6.94	0.00	0.01	0.00	2.86	0.34		
R9 tap water GC	—	—	—		6.49	0.00	0.26	5.06	0.01	0.04	0.00	0.00	4.65	0.14	0.05	0.03	0.24	0.90	7.23	8.71	104.80	0.22	0.01	0.00	2.89	0.36		
R10 H ₂ O _d ELGA	—	—	—		6.21	0.00	0.35	0.06	0.00	0.00	0.00	0.00	0.00	0.00	0.00	0.00	0.01	0.38	0.53	1.30	9.99	0.37	0.01	0.00	2.86	0.34		
R11 mud 2 (GSS50)	—	—	—		7.74	41.48	9.62	643.71	0.49	20.60	0.00	1.36	807.31	9.05	41.80	8.83	98.60	19.35	23.11	1.69	343.63	1.63	0.01	8.99	5.15	1.06		
R12 mud 3 (guar gum)	—	—	—		6.40	16.60	2.20	239.64	0.36	12.35	0.00	0.07	223.23	5.61	24.40	4.91	36.57	12.51	8.47	1.94	192.03	0.37	0.01	0.00	3.02	0.87		
R13 seawater/drill water	—	—	—		7.83	14.94	2.21	241.08	0.36	8.87	0.00	0.00	216.62	5.09	24.56	4.96	37.02	12.67	5.70	1.88	190.27	0.00	0.01	0.56	2.93	0.79		

Rh = Rhizon sample. ISE = ion-specific electrode, IC = ion chromatography, ICP-OES = inductively coupled plasma-optical emission spectroscopy. — = no data reported for samples with insufficient pore water volumes.



Table T7. Calculated salinity and elemental ratios of interstitial waters, Site M0067.

Core, section, interval (cm)	Type	Depth (mbsf)	Cl-based salinity	Na/Cl (mM/mM)	Ca/Cl (mM/mM)	Mg/Cl (mM/mM)	K/Cl (mM/mM)	Br/Cl (μM/mM)	B/Cl (μM/mM)	SO ₄ /Cl (mM/mM)
347-M0067A-										
1H-1, 135–140	Rh	1.38	21.50	0.89	0.03	0.10	0.02	1.60	1.22	0.009
1H-2, 135–140	Rh	2.88	21.12	0.98	0.03	0.10	0.03	1.60	1.26	0.005
2H-1, 33–38	Rh	3.66	18.97	1.12	0.04	0.11	0.03	1.48	1.04	0.014
347-M0067B-										
1H-1, 134–139	Rh	1.37	22.00	0.89	0.02	0.09	0.02	1.59	1.13	0.017
1H-2, 115–120	Rh	2.67	21.54	0.89	0.03	0.10	0.02	1.61	1.16	0.007
2H-1, 89–94	Rh	3.92	20.96	0.93	0.03	0.10	0.02	1.60	1.15	0.005
2H-2, 48–53	Rh	4.55	20.76	0.95	0.04	0.10	0.02	1.59	1.01	0.009
5H-1, 135–140	Rh	11.08	21.62	0.97	0.04	0.11	0.02	1.57	0.91	0.019

Rh = Rhizon sample.

Table T8. Total carbon (TC), total organic carbon (TOC), total inorganic carbon (TIC), and total sulfur (TS) in sediment, Site M0067.

Core, section, interval (cm)	Depth (mbsf)	TC (wt%)	TOC (wt%)	TIC (wt%)	TS (wt%)
347-M0067A-					
1H-2, 73–74	2.23	4.97	4.54	0.43	2.60
2H-1, 11–12	3.41	0.77	0.05	0.72	0.28
347-M0067B-					
1H-1, 40–41	0.40	7.62	6.73	0.89	2.21
1H-2, 40–41	1.89	5.10	4.63	0.47	2.34
1H-3, 34–35	3.13	5.96	5.30	0.66	2.51
2H-1, 45–46	3.45	5.58	4.93	0.66	2.76
2H-2, 41–42	4.45	0.17	0.17	0.00	0.36
4H-1, 7–8	9.57	1.20	0.02	1.18	—
5H-2, 42–43	11.62	1.10	0.02	1.08	0.22

— = below detection.

Table T9. Composite depth scale, Site M0067.

Core	Offset (m)	Top depth	
		(mbsf)	(mcd)
347-M0067A-			
1H	-0.42	0.0	-0.42
2H	-0.42	3.3	2.88
3H	-0.14	4.3	4.16
347-M0067B-			
1H	0	0.0	0.00
2H	0	3.0	3.00
4H	0	9.5	9.50
5H	0	9.7	9.70

Table T10. Splice tie points, Site M0067.

Hole, core, section, interval (cm)	Depth (mbsf)	Dept (mcd)	Hole, core, section, interval (cm)
347-		347-	
M0067A-1H-1, 116	0.75	0.75	Tie to M0067B-1H-1, 74
M0067B-1H-4, 19	3.10	3.10	Append M0067B-1H-1, 74

Table T11. Sound velocity data for lithostratigraphic units, Site M0067.

Unit	Thickness of unit (m)	Sound velocity (m/s)*	TWT (ms)	Depth (m)	Depth (mbsf)
Seafloor	23.0	1475	0.031	23.0	0.0
I	4.4	1492	0.037	27.4	4.4
II	4.6	1700†	0.045	33.9	10.9

* = sound velocities are based on values measured during the OSP. † = no direct data, data are based on Site Survey Report estimates. TWT = two-way traveltime.